Size-Transformable Nanostructures: From Design to Biomedical Applications

Xiaodong Zhang, Xiaokai Chen, Jun Song, Junmin Zhang, Xiangzhong Ren,* Yanli Zhao**

Dr. X. D. Zhang, Prof. J. M. Zhang, Prof. X. Z. Ren

International Joint Research Center for Molecular Science, College of Chemistry and Environmental Engineering, Shenzhen University, Shenzhen 518060, China.

Dr. X. D. Zhang and Prof. J. Song

College of Physics and Optoelectronic Engineering, Shenzhen University, Shenzhen 518060, China

Dr. X. D. Zhang and Prof. Y. L. Zhao

Division of Chemistry and Biological Chemistry, School of Physical and Mathematical Sciences, Nanyang Technological University, 21 Nanyang Link, Singapore 637371, Singapore

Dr. X. K. Chen

State Key Laboratory of Bioelectronics, School of Biological Science and Medical Engineering, Southeast University, Nanjing 210096, China

E-mail: zhaoyanli@ntu.edu.sg, zhangjm@szu.edu.cn, renxz@szu.edu.cn

Abstract

The size of nanostructures (NSs) strongly affects their chemical and physical properties and further impacts their actions in biological systems. Both small and large NSs possess respective advantages for disease theranostics, and this therefore presents a paradox when choosing NSs

with suitable sizes. To overcome this challenge, size-transformable NSs have emerged as a powerful tool, as they can be manipulated to possess the merits of both types of NSs. In this review, various strategies to construct size-transformable NSs are summarized, and the recent research progress regarding their biomedical applications, particularly within the fields of cancer and bacterial theranostics, is highlighted. This review will inspire researchers to further develop various methods that can be used to construct size-transformable NSs for use in novel applications within different fields.

Keywords: bacterial infection; cancer treatment; smart nanomedicine; structural transformation; theranostics

1. Introduction

Nanotechnology is one of the fastest-growing scientific fields, and is broadly applicable for biomedical uses owing to the distinct properties of nanostructures (NSs).[1] Size is one of the most important factors that determine the functions of NSs, as it significantly influences their chemical and physical properties and further impacts their actions in biological systems.[2] For example, Chithrani *et al*. found that gold nanoparticles (AuNPs) with a size of 50 nm were more easily internalized into mammalian cells than were AuNPs of other sizes (14, 30, 74, and 100 nm).[3] Jiang *et al*. demonstrated that gold and silver nanoparticle-mediated cellular responses were size-dependent.[4] Wang *et al*. reported that the size of micelles significantly influenced their blood circulation time, tumor accumulation, and tumor penetration.[5] Additionally, nanoparticles exhibited size-dependent antibacterial activity and biofilm penetration properties.[6]

Typically, small NSs possess the advantages of (1) high surface-to-volume ratio that provides them with a large surface by which to contact the biological environment,[6b] (2) excellent biosafety and biocompatibility owing to their ease of excretion from living systems,[7]

(3) capability to cross intracellular or *in vivo* barriers such as cell nuclear membranes[8] and blood-brain barriers (BBBs)[9] that allows them to enter these difficult-to-reach regions, and (4) strong penetration ability to reach the depths of solid tumors[10] and bacterial biofilms.[11] In comparison, large NSs typically exhibit long tissue retention periods[12] and slow exocytosis rates from the cells[13], both of which are ideal for long-term imaging and effective treatment. Moreover, certain large NSs possess more favorable properties than do small ones in regard to enhanced theranostics.[14] To achieve satisfactory theranostic performance in addition to acceptable biosafety, NSs should exhibit the merits of both small and large NSs, and these merits include long-term retention, deep penetration, and rapid clearance.

Among the various strategies used for overcoming the size paradox, utilizing size-transformable NSs has been demonstrated to be an available and effective method, as these types of NSs can easily integrate the advantages of small and large NSs. They can behave as small NSs for tissue penetration, rapid clearance, and crossing biological barriers, and can act as large NSs to meet the demands of long-term retention at the targeted sites. During or after the size transformation in these NSs, the loaded drugs within the NSs can be exposed or released from the system, ultimately enabling the transformable NSs to provide a versatile platform for disease theranostics.

Based on their superior properties, a great deal of progress in regard to the design and applications of size-transformable NSs has occurred over the last several decades.[15] In this review, we focus on summarizing the design methods and biomedical applications of two types of size-transformable NSs, specifically the size-decreasing and size-increasing NSs. In addition to the NSs that utilize a single-step transformation, NSs that undergo multiple transformations are also introduced. All NSs were nanosized or microsized before and after the transformation. NSs that can transform into small molecules (degradable nanoparticles)[16] and small molecules that can self-assemble *in situ* into NSs[17] have been widely summarized in other papers and

thus are excluded from the present review.

2. NSs that can Transform into Small NSs

2.1. Design

To date, much effort has been devoted to the construction of NSs that can transform into small ones. Size-decreasing NSs can typically be divided into three categories that include (1) the NSs containing or composed of small NSs that can be separated from the original systems (**Figure 1a–d**), (2) shrinkable NSs possessing stimulus-responsive hydrophilicity and hydrophobicity (**Figure 1e**), and (3) the NSs that undergo reassembly in response to stimulus triggering (**Figure 1f,g**). Various internal and external stimuli, including pH, enzymes, reactive oxygen species (ROS), glutathione (GSH), lactate, hypoxic environment, and light, have been used to trigger the transformation of these NSs.

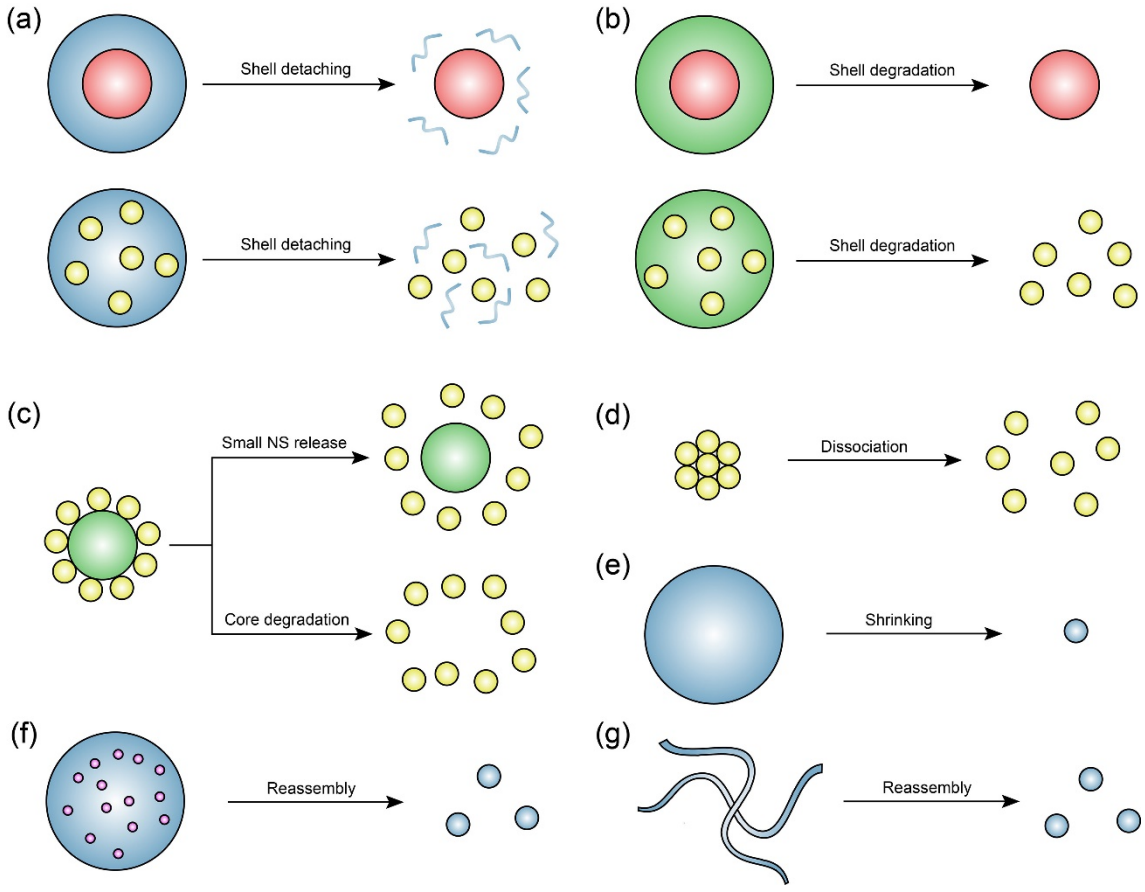

Figure 1. (a–g) Schematic illustration for the design of NSs that can transform in size from large to small.

2.1.1. Small NSs with Detachable Shells

Adding a shell can change a small NS into a large one. If the hydrophilicity of the polymers constituting the shell increases after stimulus triggering, the shell can be detached, and the encapsulated small NSs are then exposed to allow for the transformation of a large NS into a small NS (**Figure 1a**). For example, Chen *et al*. designed a core-shell polymeric NS with a shell thickness of ~50 nm that comprised pH-sensitive dimethylmalic anhydride (DMMA)-modified methoxy poly(ethylene glycol)-*block*-poly(*L*-lysine) (termed as $mPEG_{113}$-*b*-PLL_{25}/DMMA).[18] When the NSs reached the tumor environment, the weakly acidic conditions increased the hydrophilicity of $mPEG_{113}$-*b*-PLL_{25}/DMMA, subsequently leading to the disassembly of the shell and a remarkable reduction in the NS size from approximately 145 to 40 nm.

Additionally, multiple small NSs can be encapsulated into one nanocapsule during shell formation. Tseng *et al*. reported the preparation of a hypoxia-responsive carrier using the self-assembly of 6-(2-nitroimidazole)hexylamine-conjugated hyaluronic acid (HA) into which adeno-associated virus serotype 2 (AAV2)-conjugated ultrasmall iron oxide nanoparticles and lactate oxidase (LOX) were loaded.[19] Lactate within the tumor microenvironment could enter the carrier and be oxidized by LOX to increase the hypoxia level in the carrier, ultimately converting 6-(2-nitroimidazole)hexylamine into a hydrophilic moiety. As a result, the carrier dissociated, and the loaded small iron oxide nanoparticles were released.

2.1.2. Small NSs Encapsulated into Degradable Shells

Using degradable shells to encapsulate NSs can also enlarge the size of small NSs. Additionally, the degradation of the shells can promote the release of loaded small NSs from

the large NS (**Figure 1b**). For example, Hu *et al*. utilized a shell composed of NO donor-modified HA (HN) to load ultra-small dendrimeric particles into a large NS.[20] The degradation of the HA shell caused by the overexpressed hyaluronidase (HAase) within the tumor significantly decreased the size of the NSs. Similarly, Cong *et al*. reported an intracellular size-transformable nanosystem composed of small NSs (<30 nm) decorated with folic acid- and dopamine-functionalized HA.[21] These nanosystems remained large (~130 nm) during blood circulation and were predominantly internalized by cancer cells *via* the HA- and folic acid-mediated pathway. This was followed by the release of small NSs within the cells due to the degradation of HA resulting from the high level of HAase present within the cancer cells.

In addition to HA, gelatin is also a widely used polymer for loading small NSs, as it is low-cost and can be degraded by matrix metalloproteinase-2 (MMP-2) and MMP-9. Qi *et al*. used cystamine-modified gelatin to simultaneously encapsulate doxorubicin (DOX) and Fe_3O_4 nanoparticles (~11 nm), resulting in DOX-Fe_3O_4@gelatin with a large size of ~320 nm.[22] The gelatin shell could be destroyed within the acidic tumor environment due to high levels of GSH and MMP, ultimately releasing the loaded small Fe_3O_4 nanoparticles for localized cancer treatment.

2.1.3. Small NSs Added onto the Surface of an NS Core

This type of nanosystem typically contains a NS core that is surrounded by numerous small NSs at the surface. To transform these large nanosystems into small NSs, two strategies have been developed. These include (1) cleaving the linkages between the core and the covered small NSs and (2) destroying the core (**Figure 1c**). For example, Li *et al*. designed a smart polymeric nanoparticle composed of poly(ε-caprolactone) (PCL), poly(ethylene glycol)-*block*-PCL (PEG-*b*-PCL), and platinum (Pt) prodrug-conjugated poly(amidoamine)-*graft*-PCL (PCL-CDM-PAMAM/Pt) possessing an initial size of ~100 nm with small PAMAM/Pt NSs coated onto the

surface of the system.[23] As PAMAM/Pt is linked to 2-propionic-3-methylmaleic anhydride (CDM) *via* acid-labile amide bonds, the tumor acidity could trigger the release of small-sized PAMAM/Pt.

To construct a core-degradable system, Wong *et al*. used a degradable gelatin nanoparticle as the core, and they conjugated PEGylated quantum dots (~10 nm) onto the surface *via* amine-carboxyl reactions to form large nanosystems possessing a large size of ~100 nm.[24] When the core was degraded due to the large amount of MMP present within the tumor, the covered small quantum dots were subsequently released from the nanosystems. Similarly, Ruan *et al*. prepared small AuNP-coated gelatin nanoparticles, where the size could decrease from 186 to 71 nm in the presence of MMP-2.[25]

2.1.4. Dissociable Aggregates Formed by Small NSs

Some small-sized particles can form a larger NS that can dissociate under specific conditions. This strategy can significantly decrease the size of the nanoparticles from tens to hundreds of nanometers to only several nanometers (**Figure 1d**). Human serum albumin (HSA) possesses a diameter of several nanometers and has attracted much attention as a versatile platform for disease theranostics due to its inherent excellent biocompatibility and extraordinary binding capacity for various drugs. Moreover, it was observed that modified HSA can assemble into large NSs that are capable of dissociating into small ones. Chen *et al*. reported that the co-assemblies composed of paclitaxel, catalase, chlorine e6 (Ce6), and HSA exhibited a concentration-dependent dissociation ability, indicating that the co-assemblies possessed a large size of 50–100 nm during blood circulation due to their high concentration and then could be gradually be broken up into small albumin-drug complexes upon dilution after entering the tumor.[26] Recently, Cai *et al*. synthesized carboxylesterase (CE)-responsive tetrachloroperylene monoimide (P1) that could be assembled with folate-modified HSA into a

nanocluster (FHP) possessing a diameter of ~100 nm.[27] The CE within the tumor could hydrolyze P1 in the FHP, thus causing the FHP to disassemble into ultra-small particles possessing a size of ~10 nm. Additionally, HSA-coated NSs have been reported to exhibit stimulus-responsive size changeability. Guo *et al.* found that bismuth sulfide nanorods (BiS NRs) could form large aggregates after modification with HSA and docetaxel.[28] Following laser irradiation, the heat generated from the BiS NRs could cause severe thermal stress within the NS, ultimately leading to the disassembly of the system.

Similar to HSA, dendrimers are commonly employed as the moieties of small-sized particles, as they are modifiable, facile to load with drugs, and easy to obtain. For example, Ray *et al*. conjugated hyperbranched polyester polyol with linear polycarbonate and then grafted this structure with pH-sensitive *N*,*N*′-dibutylethylenediamine (DBA).[29] Large NSs possessing hydrodynamic diameters of 150–190 nm could be formed at neutral pH *via* the aggregation of the obtained copolymers, and these structures could be dissociated into smaller NSs with diameters ranging from 3 to 5 nm under acidic conditions due to the protonation of tertiary amine groups in DBA.

In addition to self-assembly, HSA- and dendrimer-based macromolecules can be crosslinked *via* stimulus-responsive linkers to form dissociable NSs. Yang and coworkers constructed hypoxia-responsive nanosystems based on the crosslinking between Ce6-conjugated HSA and oxaliplatin prodrug-conjugated HSA *via* hypoxia-sensitive azobenzene groups.[30] These nanosystems possessed a size of 100–150 nm under normal oxygen partial pressure, and they rapidly transformed into ultra-small NSs with a diameter of less than 10 nm in the hypoxic tumor microenvironment. Similarly, Guo *et al*. used a mild-acid-responsive linker (1,6-bis[4-formylbenzoyloxy] hexane) to crosslink dendrigraft poly-*L*-lysines, and the obtained structure underwent an acid-triggered size change from 123 to ~10 nm.[31]

2.1.5. Shrinkable NSs

Amphiphilic polymers can assemble into polymeric NSs. If the hydrophobicity or hydrophilicity of the polymers changes under stimulus triggering, the size of the assemblies may be transformed (**Figure 1e**). Generally, increasing the hydrophobicity and decreasing the hydrophilicity of the polymers can induce a size decrease in the polymeric NSs. Thus, to transform the large NSs into small ones, the polymer that constitutes the large NSs usually contains a cleavable hydrophilic moiety.

Wang *et al*. employed GSH-responsive disulfide bonds to link PAMAM dendrimers and then further modified them with cell-penetrating peptides.[32] The hydrodynamic size of the polymer assemblies was ~100 nm, and the size decreased to ~50 nm when the intramolecular disulfide bonds were cleaved by the intracellular GSH possessing strong reducibility. In another case, shrinkable nanoparticles were synthesized by Guo *et al*. using a polymer consisting of an amphiphilic polymer PCL-PEG conjugated with another hydrophilic PEG segment *via* an enzyme-responsive peptide.[33] When the peptide linker was cleaved by proteases, the outer hydrophilic peptide-PEG component was shielded, thus enabling the size of the assemblies to gradually decrease from 218 to 79 nm after incubation for 24 h.

2.1.6. Stimulus-Responsive Molecule-Doped NSs

In addition to the above-mentioned strategies, doping stimulus-responsive molecules during the assembly can also affect the self-assembly process. The molecules can induce the reassembly of systems after stimulus triggering, thus endowing the obtained NSs with size-decreasing ability (**Figure 1f**). Recently, Chen *et al*. doped a photodegradable indocyanine green (ICG) molecule into assemblies (SiPINGs) possessing a relatively large diameter of ~39 nm that were composed of organosilica nanodots and methoxypoly(ethylene glycol)-*block*-poly(*L*-glutamic acid sodium salt) (PEG–PLE).[34] When the ICG molecule was replaced by its

photodegraded product (dICG) or the ICG molecule in the assemblies was degraded into dICG after laser irradiation, reassembly of the structures occurred, ultimately leading to a decrease in their size down to ~11 nm. As a result, the assemblies act as a photocontrolled size-decreasing nanosystem.

2.1.7. Transformation from Nanofibers to Nanospheres

Nanofibers typically possess a long size in one dimension and are easy to form into net-like structures within biological systems. Thus, the transformation from nanofibers to nanospheres is also a strategy that can change large NSs into small NSs (**Figure 1g**). Chen *et al*. modified tetraphenyl-substituted azadipyrromethene-BF_2 with hydrophobic dodecyloxy groups on one side and two hydrophilic triethylene glycol chains on the other side.[35] The obtained amphiphilic compound (aza-BODIPY-1) could self-assemble into fiber-like micellar structures possessing a diameter of ~27 nm and a length of ~600 nm through J-aggregation. Under NIR light irradiation, the photothermal effect of the dye molecules contributed to the increasing temperature. When the temperature was elevated past the phase transition temperature of aza-BODIPY-1, the sharp J-aggregation band in the nanofibers nearly disappeared, ultimately leading to the transformation from nanofibers into nanospheres possessing a small diameter of ~20 nm.

2.2. Applications

2.2.1. Enhanced Tumor Penetration

To allow efficient tumor accumulation through the enhanced permeability and retention (EPR) effect, the size of the NSs should be in the range of 40–200 nm. This is due to the ability of larger NSs to be easily internalized by the reticuloendothelial system, while smaller NSs are rapidly excreted through the kidney.[36] However, NSs in this size range exhibit poor tumor

penetration and distribution due to the presence of dense extracellular matrices, high cell packing density, increased interstitial flow pressure, and slow interstitial flow velocity within the tumor matrix.[37] NSs that can change from large to small NSs are ideal for solving the above-mentioned problems, as they can possess a relatively large size during blood circulation for effective accumulation in the tumor. Meanwhile, after size transformation in the tumor region, they are relatively small and thus suitable for further tumor penetration.

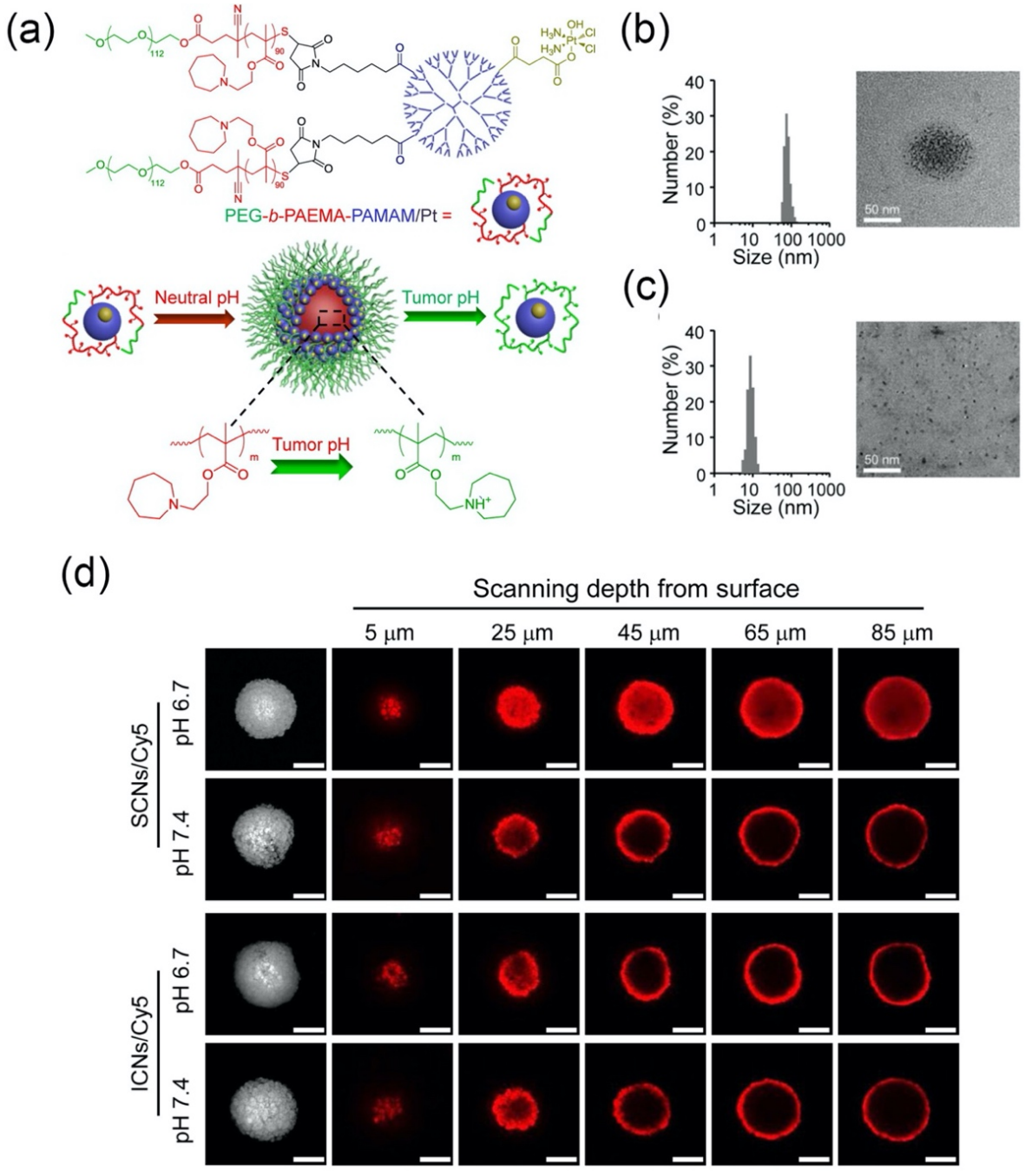

Figure 2. (a) Schematic representation showing the preparation of pH-sensitive SCNs/Pt and their transformation into small NSs triggered by the acidic pH of the tumor. (b,c) Dynamic light scattering (DLS) results and transmission electron microscopy (TEM) images of SCNs/Pt at (b) neutral pH and (c) acidic pH. (d) Confocal fluorescence images showing the penetration performance of Cy5-labeled SCNs (SCNs/Cy5) and ICNs (ICNs/Cy5) in BxPC-3 MCSs. Reprinted with permission.[38] Copyright 2016, American Chemical Society.

For example, Li *et al*. used the amphiphilic polymer PEG-*block*-poly(2-azepane ethyl methacrylate) (PEG-*b*-PAEMA) to modify platinum-prodrug conjugated PAMAM dendrimers (PAMAM/Pt), and the obtained PEG-*b*-PAEMA-PAMAM/Pt self-assembled into pH-sensitive cluster nanobombs (SCNs) with an initial size of ~80 nm under neutral conditions (**Figure 2a,b**).[38] The hydrophobic PAEMA moieties in SCNs could be protonated to become hydrophilic in the acidic tumor environment, thus leading to the instantaneous disintegration of the big assemblies into small dendrimer-based building blocks (< 10 nm) (**Figure 2c**). To evaluate the tumor penetration ability of the NSs, BxPC-3 human pancreatic cancer cell-derived multicellular spheroids (MCSs) were used. Confocal fluorescence imaging results showed that Cy5-labeled SCNs (SCNs/Cy5) exhibited deeper tumor penetration and more uniform distribution within the tumor at acidic pH (pH = 6.7) compared to that in a neutral environment (pH = 7.4) (**Figure 2d**). This was attributed to their rapid dissociation into small particles under acidic conditions. For pH-insensitive cluster nanostructures (ICNs) that could not disintegrate into small particles, Cy5-labeled ICNs were primarily distributed on the surface of MCSs and were difficult to observe in the center of MCSs at both acidic and neutral pH.

A previous study reported that fiber-shaped micelles could exhibit longer circulation periods than those of their spherical counterparts.[35] However, similar to large nanospheres, it is difficult for these nanofibers to achieve deep penetration in the tumor due to the above-

mentioned obstacles. To simultaneously achieve long-term circulation and enhanced tumor penetration, amphiphilic aza-BODIPY-1 was used to self-assemble into temperature-sensitive nanofibers (1-NFs) that could transform into sphere-shaped nanoparticles (1-NPs) after the temperature was elevated past the phase transition temperature of aza-BODIPY-1.[35] The authors found that 1-NFs exhibited a 7.6 fold longer half-life of blood circulation period than that of 1-NPs. Additionally, 1-NFs exhibited comparable tumor penetration ability to that of the small 1-NPs after laser irradiation, as their intrinsic photothermal effect could cause a temperature increase that resulted in the transformation of 1-NFs to 1-NPs.

2.2.2. Enhanced Bacterial Biofilm Penetration

Bacterial biofilms consisting of well-organized bacterial communities encased in an extracellular matrix of biomolecules display high levels of antibiotic tolerance based on the inability of antibacterial agents to penetrate into the full depth of the biofilms.[11a] Nanoparticles can be used to load antibiotics to achieve effective drug accumulation in bacterium-infected tissues, as these sites exhibit enhanced permeability and retention effects for nanoparticles.[39] Despite these advantages, it is difficult to determine the size of the nanoparticles as large nanoparticles are difficult to deeply penetrate into the biofilms,[6c] while small nanoparticles exhibit short blood circulation time. Thus, it is highly desirable to develop size-changeable NSs that can simultaneously achieve long circulation times and enhanced biofilm penetration.

Gao *et al*. prepared size- and charge-transformable azithromycin (AZM)-conjugated clustered nanoparticles (AZM-DA) through electrostatic complexation between AZM-conjugated poly(amidoamine) dendrimers (PAMAM-AZM) and 2,3-dimethyl maleic anhydride (DA)-modified poly(ethylene glycol)-*block*-polylysine (PEG-PLys-COOH[DA]) (**Figure 3a**).[40] The AZM-DA nanoparticles exhibited a long circulation time due to their suitable size (112.0 nm) and negative surface charge (−2.2 mV) at neutral pH (**Figure 3b**).

Moreover, they could disassemble in the acidic biofilm microenvironment (pH 6.0) due to the pH-sensitivity of the DA moiety, and subsequently released small-sized and positively charged PAMAM-AZM nanoparticles. Compared to pH-insensitive control nanoparticles (named as AZM-SA) that could not dissociate into small nanoparticles, AZM-DA nanoparticles exhibited enhanced biofilm penetration and accumulation ability as well as excellent antibiofilm activity (**Figure 3c–h**).

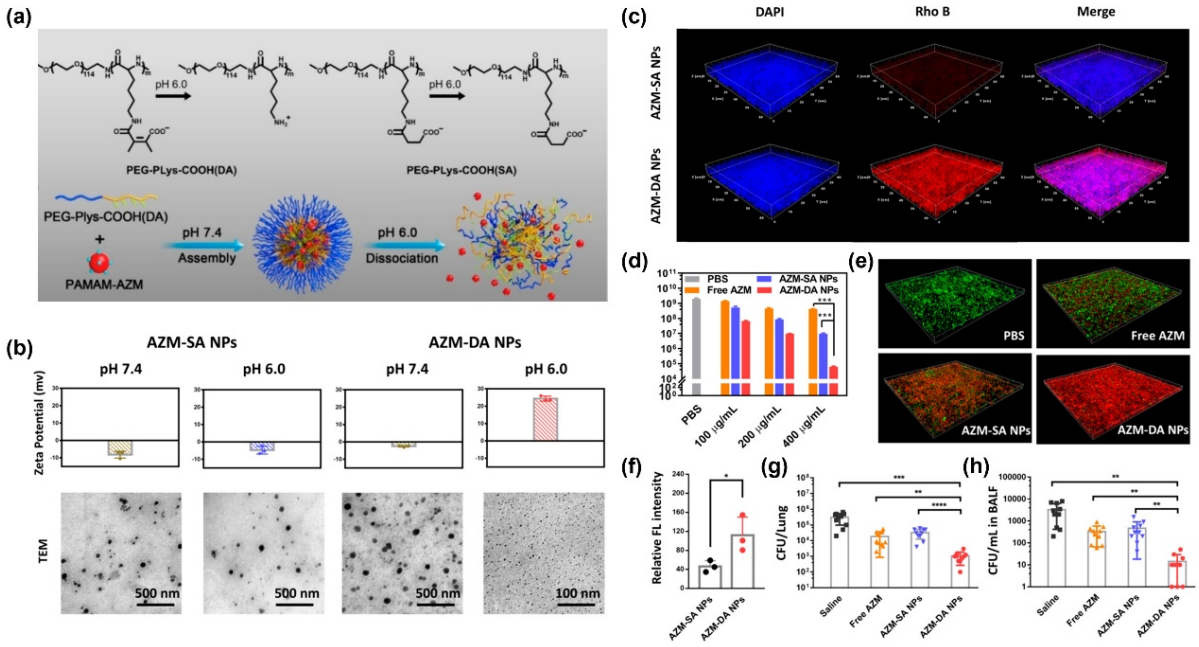

Figure 3. (a) Structures of DA- and SA-modified PEG-*b*-PLys and a schematic illustration of the self-assembly of AZM-DA nanoparticles that can release small PAMAM-AZM nanoparticles into the acidic biofilm microenvironment. (b) Zeta potentials and TEM images of AZM-DA nanoparticles and AZM-SA nanoparticles after incubating at pH 7.4 or pH 6.0 for 2 h. (c) 3D-reconstructed confocal fluorescence images of *Pseudomonas aeruginosa* (*P. aeruginosa*) biofilms after incubation with rhodamine B (Rho B)-labeled AZM-DA nanoparticles or AZM-SA nanoparticles (blue fluorescence: *P. aeruginosa* biofilms stained by 4',6-diamidino-2-phenylindole [DAPI]; red fluorescence: Rho B). (d) Antibacterial performance of various drugs in *P. aeruginosa* biofilms. (e) Live/dead staining results of *P. aeruginosa* biofilms after various treatments for 12 h. Live and dead bacteria were stained with

green fluorescent SYTO 9 and red-fluorescent propidium iodide (PI), respectively. (f) *Ex vivo* imaging fluorescence intensity of lungs excised from mice at 24 h post intravenous injection with AZM-DA nanoparticles or AZM-SA nanoparticles. (g,h) Bacterial amounts in the lung (g) and lung bronchoalveolar lavage fluid (BALF) (h) after receiving different treatments. Reprinted with permission.[40] Copyright 2020, American Chemical Society.

2.2.3. Controlled Drug Release

Chemotherapy, one of the standard cancer treatments, is typically accompanied by serious side effects due to the undesired accumulation of chemotherapeutic agents in normal tissues. Using a nanocarrier to load chemotherapeutic agents is considered as a method to alleviate the side effects of chemotherapeutic agents, as the nanocarrier can promote drug accumulation in tumors and reduce drug content in normal tissues. Additionally, rapid drug release from carriers during blood circulation may still lead to severe side effects, while slow drug release in the tumor cannot effectively eliminate the tumors. As a result, it is desirable to develop stimulus-responsive drug delivery systems to provide accurate cancer therapy. For NSs that can change from large to small ones, the loaded drugs in the system can be released in a controlled manner during the transformation.

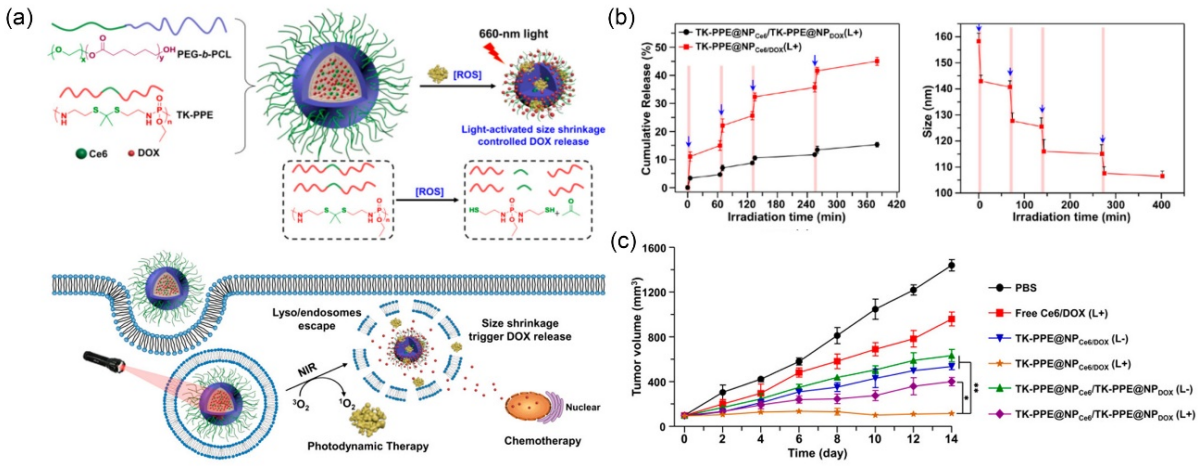

Figure 4. (a) Schematic illustration detailing the preparation of TK-PPE@$NP_{Ce6/DOX}$ that can transform from large to small NSs after light irradiation and their application in light-triggered drug release. (b) Laser-triggered drug release profiles from TK-PPE@$NP_{Ce6/DOX}$ and its size change. Blue arrows indicate that the laser is on. (c) Relative tumor volumes of the mice after various treatments. Reprinted with permission.[41] Copyright 2018, American Chemical Society.

Cao *et al*. prepared smart NSs (TK-PPE@$NP_{Ce6/DOX}$) that exhibited light-activated size shrinkage, and these NSs were comprised ROS-responsive poly(thioketal phosphoester) (TK-PPE), amphiphilic diblock copolymer PEG-*b*-PCL, photosensitizer Ce6, and DOX (**Figure 4a**).[41] Laser irradiation could promote ROS generation from the encapsulated Ce6 molecule, which cleaved the TK linker *in situ* and resulted in size reduction. Meanwhile, the loaded drug DOX was quickly released from the system under laser irradiation in conjunction with decreasing nanoparticle size (**Figure 4b**), which was attributed to the generated ROS that destroyed the core of the system. In comparison, the separate encapsulation system (TK-PPE@NP_{Ce6}/TK-PPE@NP_{DOX}) could not quickly release DOX under the same conditions, as the generated ROS in the TK-PPE@NP_{Ce6} system could not dissociate the core of the TK-PPE@NP_{DOX} system. Thus, TK-PPE@$NP_{Ce6/DOX}$ exhibited excellent anticancer performance after laser irradiation (**Figure 4c**). As stated above, the designed photo-controlled size-shrinkable nanosystems (SiPINGs) could be used to load the anticancer drug DOX, thus forming DOX@SiPINGs.[34] The encapsulated DOX was difficult to release from the system without laser irradiation due to the strong interactions between DOX and SiPINGs. However, massive and rapid drug release could be achieved during the transformation of the system that was triggered by 808 nm laser irradiation.

2.2.4 Promoted Cell Nucleus Influx

The cell nucleus functions as the brain of the cell, as it contains the majority of the cellular genetic materials. The nucleus of cancer cells is typically the ultimate target of most chemotherapeutics such as DOX, cisplatin, and camptothecin. Moreover, nucleus-targeted cancer therapies typically exhibit higher efficacy than other organelle-targeted remedies.[42] To enter the cell nucleus, NSs should possess a small size of less than 40 nm[43] owing to the ultra-small size of nuclear pores, as these are the channels that NSs must pass through. To simultaneously achieve effective tumor accumulation and improve the intranuclear drug delivery efficiency, NSs should have a relatively large size during blood circulation and then transform into small-sized NSs before entering the cell nuclei.

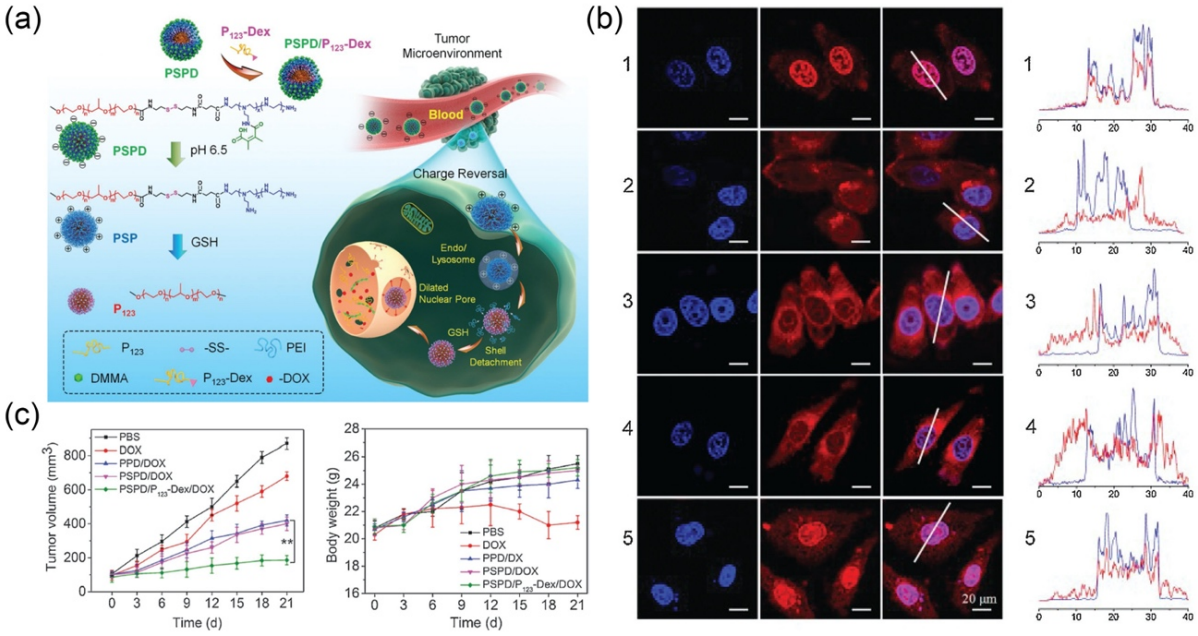

Figure 5. (a) Schematic illustration for the fabrication of PSPD/P_{123}-Dex/DOX and its application in nucleus-targeted drug delivery. (b) Confocal fluorescence images and line-scan fluorescence intensity profiles of the cells after incubation with free DOX and DOX-loaded micelles at the same DOX concentration. Blue and red fluorescence signals were derived from the cell nuclear staining dye 4',6-diamidino-2-phenylindole and the anticancer drug DOX, respectively. The numbers 1–5 represent free DOX, PPD/DOX, PSPD/DOX, PPD/P_{123}-Dex/DOX, and PSPD/P_{123}-Dex/DOX, respectively. (c) Relative tumor volumes and body

weights of the mice after various treatments. Reprinted with permission.[44] Copyright 2017, Wiley-VCH.

Wang *et al*. constructed a polymeric NS composed of amphiphilic poly(ethylene glycol)-*block*-poly(propylene glycol)-*block*-poly(ethylene glycol) (P_{123}) linked to charge-reversible DMMA-polyethylenimine (PEI) *via* disulfide bonds (termed as PSPD), dexamethasone (Dex)-conjugated P_{123}, and the anticancer drug DOX (**Figure 5a**).[44] The prepared core-corona NS (named as PSPD/P_{123}-Dex/DOX) possessed a uniform size of ~120 nm and a negative charge at physiological pH. After reaching the tumor regions, the transition of the β-carboxylic acid group to an amine group at the weakly acidic pH could induce a charge reversal of the micelles and enhance charge-mediated endocytosis. Then, the disulfide bonds in the intracellular micelles were broken by GSH, resulting in the detachment of hydrophilic PEI from the system and triggering a size reduction from ~120 to 30 nm. Furthermore, the glucocorticoid receptor-targeting Dex moiety within the NS could promote nuclear targeting and nuclear pore dilation. Therefore, both *in vitro* and *in vivo* results revealed that PSPD/P_{123}-Dex/DOX could achieve effective intranuclear drug delivery and exhibited good tumor inhibition, while free DOX and other micelles composed of GSH-insensitive P_{123}-DMMA-PEI without disulfide bonds (PPD) or Dex-free micelles exhibited low nuclear accumulation ability and poor anticancer efficiency (**Figure 5b,c**).

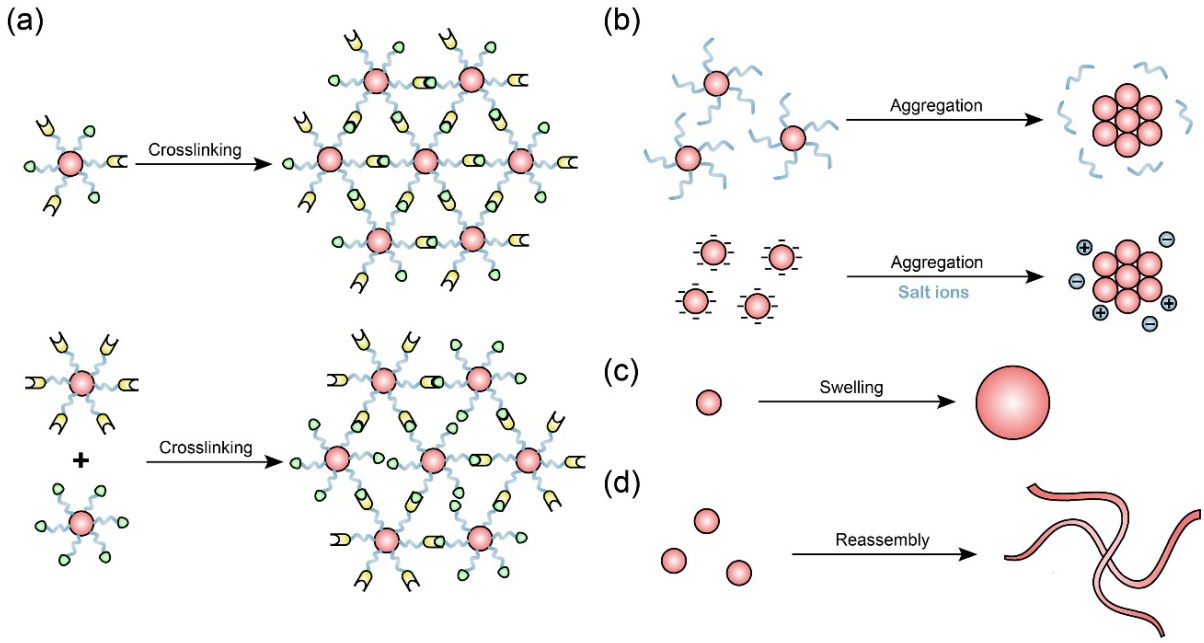

Figure 6. (a–d) Schematic illustration for the design of NSs that can transform in size from small to large NSs.

3. NSs that can Transform into Large NSs

3.1. Design

Similar to the size-decreasing NSs, the NSs that can change from small to large ones are classified into three categories; however, their design routes are different than those of size-decreasing NSs. The size-increasing NSs include (1) the NSs that can be used to constitute large NSs (**Figure 6a,b**), (2) expansile NSs that can swell due to increasing hydrophilicity (**Figure 6c**), and (3) the NSs in which reassembly occurs after stimulus triggering (**Figure 6d)**.

3.1.1. Crosslinkable NSs

Crosslinking of nanoparticles is a widely used strategy to increase the size of NSs (**Figure 6a**). Based on the interaction between the crosslinked nanoparticles, the crosslinking methods can be classified into chemical methods (in which chemical bonds are used to crosslink the nanoparticles) and physical methods (in which physical interactions such as host–guest

interactions, positive–negative charge interactions, and complementary base interactions are used). To avoid undesired crosslinking in healthy tissues, a number of efforts have been made to control the crosslinking of these nanoparticles, and strategies such as the incorporation of cleavable moieties to protect one or both of the reacted groups and the use of external stimuli to control the crosslinking process have been developed.

Crosslinking via chemical bonds: The presence of enzymes may trigger or promote certain specific chemical reactions. As a result, the controlled release of enzymes can be used to regulate the process and rate of crosslinking *via* chemical reactions. Taking advantage of the strong catalytic activity of transglutaminase (TG) that can promote the formation of isopeptide bonds between the amine groups and acyl groups, Hu *et al*. designed a core−shell based nanogel (CS-NG) that contained the core nanogel (C-NG), TG-encapsulated shell nanogel (S-NG), and HSA decorated on the surface of C-NG.[45] The shell composed of HA could be degraded by the overexpressed HAase within the tumor, and the nanogel then released the encapsulated TG and formed crosslinked structures by catalyzing the reactions between the amine groups and acyl groups of HSA.

In addition to the two reacted groups in one type of nanoparticle, nanosystems composed of two types of nanoparticles that each possess one of the reactive groups have also been designed. Ruan *et al*. fabricated nanosystems (named as AuNP-A&C) comprised of Ala-Ala-Asn-Cys-Lys modified AuNPs (AuNPs-AK) and 2-cyano-6-aminobenzothiazole-modified AuNPs (AuNPs-CABT).[12a] The AK moieties on the surface of AuNPs could be hydrolyzed to expose the 1,2-thiolamino group in the presence of tumor-overexpressed legumain, and these could then react with the contiguous cyano group on AuNPs-CABT, ultimately resulting in the crosslinking of the two kinds of AuNPs.

Crosslinking via host–guest assembly: Due to their reversibility and adaptability,[46] host–guest interactions can also be used to construct crosslinkable NSs. Using the strong host–guest

interactions between β-cyclodextrin (β-CD) and ferrocene (Fc), Wang *et al*. constructed mono-6-thio-β-CD (β-CD-SH)-modified AuNPs and Fc-functionalized PEG (Fc-PEG-Fc).[47] The Fc in Fc-PEG-Fc was first oxidized into ferrocenium cations (Fc^+) by anhydrous ferric chloride so that it could not interact with β-CD. Upon reaching the tumor region, Fc^+ would be reduced to Fc by the overexpressed GSH and could then form inclusion complexes with β-CD on the surface of AuNPs, ultimately leading to the crosslinking of the AuNPs.

Crosslinking via positive – and negative charge interactions: The surface charge is typically present to stabilize the nanoparticles, and nanoparticles that possess a strong positive charge can crosslink with those that possess a negative charge. Nam *et al*. synthesized positively charged amine group-functionalized AuNPs and then modified a pH-sensitive citraconic amide moiety-containing molecule to reverse the surface charge of the AuNPs.[48] The citraconic amide moiety was stable under neutral or basic conditions; however, it tended to hydrolyze and produce citraconic acid at a pH lower than 7.0. Thus, the surface molecule could become positively charged as the terminal functional group changed from a carboxylate anion to a protonated amine group. Then, the unhydrolyzed AuNPs with a negative charge could crosslink with the hydrolyzed AuNPs that possess a positive charge.

Crosslinking via complementary base pairing: Single-stranded DNA can selectively bind to its complementary strand. Based on this principle, Yang *et al*. designed MMP-responsive nanosystems containing two types of AuNPs possessing complementary DNA strands attached to their surfaces.[49] Then, the complementary DNA strands were protected by a peptide linker to allow the nanosystems to be monodispersed during circulation. Upon arrival at the MMP-rich tumor sites, the PEG layer was rapidly detached to expose the complementary DNA strands, ultimately leading to the rapid crosslinking of AuNPs driven by DNA hybridization.

3.1.2. Aggregatable NSs

The formation of nanoparticle aggregates is a feasible method to increase the size of NSs. To induce the aggregation of well-dispersed nanoparticles, two general methods have been developed. These methods include decreasing the NS hydrophilicity and screening the electrostatic effect (**Figure 6b**).

Aggregation induced by reducing hydrophilicity: The nanoparticles used for biomedical applications typically possess hydrophilic moieties that make them stable and water-dispersible under physiological conditions. If the hydrophilic moieties become hydrophobic or less hydrophilic, the nanoparticles can form aggregates. For example, Li *et al*. found that nanocomplexes composed of bovine hemoglobin and IR780 possessed an isoelectric point that was close to the pH value of the tumor microenvironment.[50] The size of the nanocomplexes significantly increased when they moved from the normal tissue possessing a neutral pH to the acidic tumor microenvironment with a pH value that was close to their isoelectric point, as the complexes were less hydrophilic in the tumor environment.

Aggregation induced by the screening electrostatic effect: Electrostatic repulsion is closely related to the colloidal stability of nanoparticles and inhibits the aggregation of nanoparticles. Sun *et al*. found that salt-containing biological media could screen the electrostatic repulsion and induce the aggregation of citrate-capped AuNPs.[51] As a result, intratumoral injection of AuNPs could form large aggregates *in situ*.

3.1.3. Expansile NSs

As stated above, the hydrophobicity and hydrophilicity of the components in the polymeric nanoparticles significantly influence their size. In addition to decreasing the size, a hydrophobicity/hydrophilicity change of the components can increase the size of the nanoparticles (**Figure 6c**). In contrast to shrinkable NSs, the components in expansile NSs

typically decrease their hydrophobicity and increase their hydrophilicity after stimulus triggering.

For example, Griset *et al*. found that the nanoparticles (eNPs) composed of polymers containing 2,4,6-trimethoxybenzaldehyde possessed a favorable expansile ability, and the hydrodynamic size increased from ~100 to ~1000 nm when the solution was changed from neutral to weakly acidic.[52] This size increase is a result of the observation that the 2,4,6-trimethoxybenzaldehyde moiety is stable at neutral pH but hydrolyzes under mildly acidic conditions (pH ~5), ultimately leading to decreased hydrophobicity of the polymers. To increase the colloidal stability and tumor-targeting ability of eNPs, they used folic acid-conjugated PEGylated lipids to encapsulate the eNPs, as these could maintain the pH-activated expandability of eNPs.[53]

Chitosan-based NSs also exhibit pH-responsive expansile ability. Fang *et al*. designed nanosystems that were formed by the crosslinking between chitosan and poly(N-isopropylacrylamide) followed by surface decoration with PEG and a breast cancer-targeting peptide.[54] The system was observed to exhibit a spherical shape with a diameter of ~100 nm at pH 7.4. When the pH value decreased to 5.3, the diameter of the nanoparticles expanded to approximately 600 nm after 12 h. The authors speculated that the changeability of the system was attributed to the protonation–deprotonation equilibrium of amino groups in chitosan. Tian *et al*. used chitosan to modify carboxylic acid-capped photoluminescent Ag_2S quantum dots.[55] The obtained NSs possessed a small size of 35–45 nm at neutral pH (pH = 7.4) and expanded to 48–100 nm at a pH value of 5.0.

Recently, Xu *et al*. obtained size-changeable micelles using the self-assembly of maleimide-terminated PEG-*block*-poly(β-amino ester) and succinic anhydride-modified cisplatin-conjugated poly(ε-caprolactone)-*block*-poly(ethylene oxide)-triphenylphosphonium.[37] The micelles were then modified with thiolated collagenase and

coated with chondroitin sulfate to form the final nanoparticles. At pH 6.8, which is close to the pH of the acidic tumor microenvironment, the hydrophobic poly(β-amino ester) segments in the nanoparticles became hydrophilic and caused an expansion of the nanoparticles from ~98 nm to 245 and 277 nm after 3 h and 6 h, respectively.

3.1.4. Transformation from Nanospheres to Nanofibers

The transformation from nanospheres to nanofibers also increased the size of the NSs (**Figure 6d**). To construct NSs that can change from nanospheres to nanofibers, the molecules that can form fibrous structures are usually further modified to form sphere-shaped particles.

Some peptides and their derivatives tend to form β-sheet α-helices, or combination of these secondary structures due to the presence of extensive intermolecular hydrogen bonds, thus enabling them to form fibrous structures.[56] Inspired by the discovery that Lys-Leu-Val-Phe-Phe (KLVFF) can form nanofibers *via* β-sheet formation,[56b] Yang *et al*. designed a peptide-based self-assembly consisting of a hydrophobic bis-pyrene (BP), KLVFF, a hydrophilic PEG, and a pH-responsive peptide (His_6).[57] The BP-KLVFF-His_6-PEG could form nanospheres *via* self-assembly in a phosphate buffer solution. When the nanospheres reached the tumor region, they could transform into nanofibers due to the altered hydrophilic/lipophilic balance induced by tumor microenvironment acidity. Similarly, FFVLK, the reverse sequence of KLVFF, can also be used to construct fiber-transformable NSs. Zhang *et al*. synthesized a transformable peptide-based monomer (TPM) containing BP, FFVLK, and a HER2-binding disulfide cyclic peptide.[58] TPM could self-assemble into sphere-shaped NSs where BP and FFVLK served as the hydrophobic core and the cyclic peptide constituted the hydrophilic shell. Upon interaction with $HER2^+$ cancer cells, the sphere-shaped NSs would transform into networks composed of fibrous NSs *in situ*.

In addition to KLVFF and its reverse sequence FFVLK, the tetrapeptide segment Gly-Gly-Gly-His (GGGH) that allows massive hydrogen bonding interactions is also an effective building block for the formation of nanofibers. Zhang *et al*. designed a smart polymer (CTGP) containing a hydrophobic 16-carbon alkyl chain for membrane anchoring and self-assembly, a tetraphenylethylene probe for fluorescence imaging, GGGH, a cathepsin B-responsive peptide sequence (Gly-Phe-Leu-Gly, GFLG) to link the above-mentioned moieties to the PEG domain, and a hydrophilic PEG moiety and a cationic peptide (Lys) to enhance water dispersity and control the self-assembly of micelles.[59] CTGP could self-assemble into sphere-shaped micelles and load the anticancer drug DOX (named CTGP@DOX). After the cleavage of the GFLG sequence by pericellular-overexpressed cathepsin B, spherical CTGP@DOX could transform into nanofibers as a result of hydrophilic–hydrophobic conversion and hydrogen bonding interactions.

Moreover, chitosan can be used to form nanofibers.[60] Based on this, Qi. *et al*. fabricated a chitosan–peptide conjugate (CPC-1) composed of a chitosan backbone, an antimicrobial peptide (CGGGKLAKLAKKLAKLAK), and a PEG-conjugated enzyme-cleavable peptide (GPLGVRGC).[61] CPC-1 could self-assemble into sphere-shaped nanoparticles in aqueous solution. After reaching the infected region, the enzyme-cleavable peptides could be detached by the bacterial gelatinase. As a result, the balance of hydrophobicity and hydrophilicity in the NSs was destroyed, leading to the reorganization of NSs into nanofibers *via* the chain-chain interactions of the chitosan component.

3.2. Applications

3.2.1. Enhanced Tumor Retention

Despite the presence of the EPR effect in the tumor, the efficacy of nanomedicine is still far from satisfactory, and this is primarily due to the low and transient accumulation of

therapeutic nanosystems within the tumor. Therefore, it is ideal to construct a nanomedicine that can exhibit long-term tumor retention, and the use of transformable NSs has been demonstrated to provide a practical method to achieve this goal.

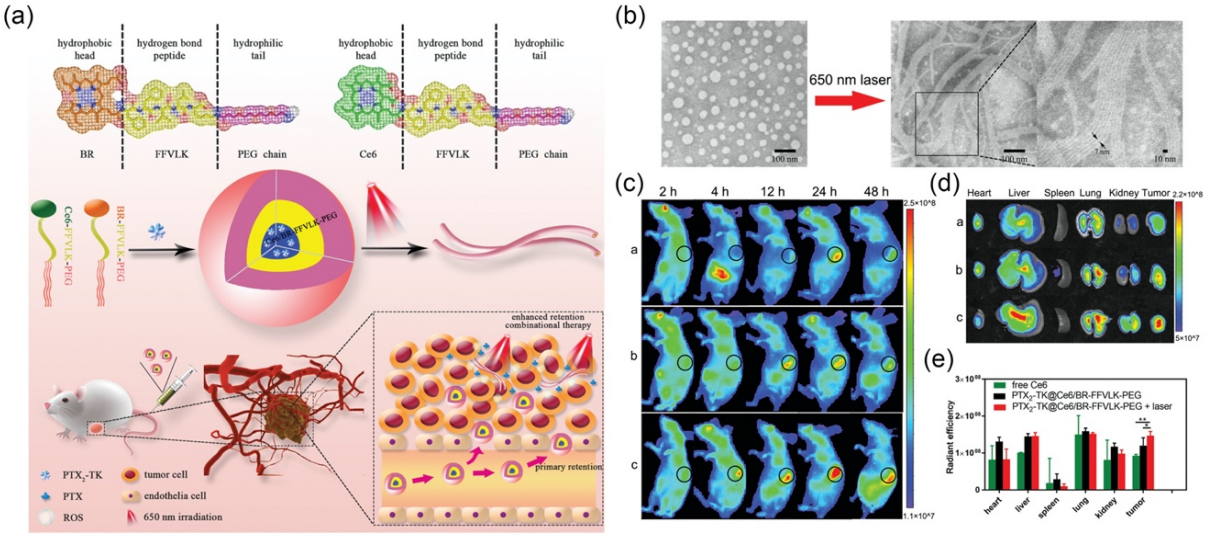

Figure 7. (a) Schematic illustration showing the design of linear chimeric triblock molecules and the transformation of PTX_2-TK@Ce6/BR-FFVLK-PEG for enhanced tumor retention. (b) TEM images of PTX_2-TK@Ce6/BR-FFVLK-PEG without and with 650 nm laser irradiation. (c) *In vivo* fluorescence images of the mice with different intravenous treatments. (d) *Ex vivo* fluorescence images of major organs and tumors from the mice after various treatments and (e) the corresponding statistical results. The letters "a", "b", and "c" represent free Ce6, PTX_2-TK@Ce6/BR-FFVLK-PEG, and PTX_2-TK@Ce6/BR-FFVLK-PEG upon the irradiation, respectively. Reprinted with permission.[62] Copyright 2019, Wiley-VCH.

For example, Liu *et al*. used the hydrophobic photosensitizer Ce6 and ROS-responsive bilirubin (BR) to modify the FFVLK-conjugated PEG chain to obtain Ce6-FFVLK-PEG and BR-FFVLK-PEG, respectively.[62] The two types of systems together could form sphere-shaped micelles (Ce6/BR-FFVLK-PEG) and were able to encapsulate paclitaxel dimers with thioketal linkers (PTX_2-TK) (**Figure 7a**). After laser irradiation, the ROS generated by Ce6 could change

hydrophobic BR into its hydrophilic analogue, ultimately leading to the reorganization of the NSs. As a result, the sphere-shaped micelles possessing a size of ~50 nm transformed into nanofibers possessing a long length (**Figure 7b**). *In vivo* fluorescence imaging results indicated that the combined treatment of laser irradiation and PTX_2-TK@Ce6/BR-FFVLK-PEG could result in long-term tumor retention due to the formation of large NSs after irradiation (**Figure 7c–e**).

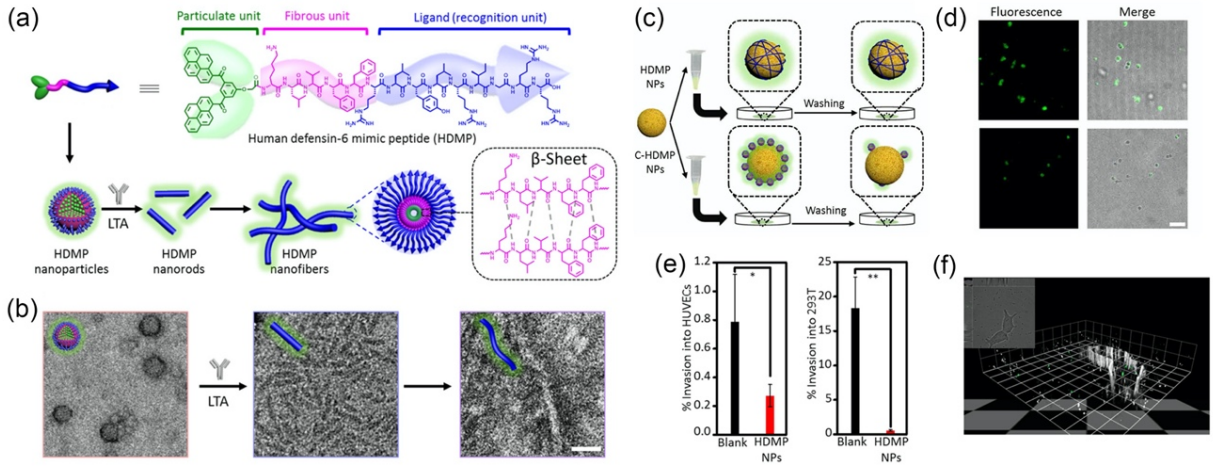

Figure 8. (a) Structure of HDMP and schematic illustration of spherical HDMP nanoparticles that can transform into nanorods and nanofibers after incubation with LTA. (b) TEM images of HDMP nanoparticles, nanorods, and nanofibers triggered by LTA at 24 and 48 hours, respectively. (d) Schematic illustration of HDMP nanoparticle- and C-HDMP nanoparticle-treated bacteria. (d) Confocal images showing the specificity of HDMP nanoparticles (top) and C-HDMP nanoparticles (bottom) to *Staphylococcus aureus* (*S. aureus*). (e) Invasion performance of bacteria to human umbilical vein endothelial cells (HUVECs) and human embryonic kidney 293 (293T) cells without (blank) and with the treatment of HDMP nanoparticles. (f) 3D confocal image of 293T cells invaded by *S. aureus*. Reprinted with permission.[63] Copyright 2020, the authors, some rights reserved; exclusive licensee American Association for the Advancement of Science.

3.2.2. Enhanced Accumulation and Retention in Bacterium-Infected Tissues

Effective accumulation and retention in infected tissues are important factors for fighting bacterial infections. Qi *et al*. reported that the transformation of the above-mentioned CPC-1 nanoparticles into fibrous NSs that was triggered by the gelatinase in the infected tissues could lead to the exposure of antimicrobial peptides for multivalent cooperative electrostatic interactions with bacterial membranes.[61] Moreover, they found that *in situ* transformation could also improve the accumulation and retention of CPC-1 in infected regions, which is beneficial for efficiently killing the bacteria. Recently, Fan *et al*. constructed a human defensin-6 mimic peptide (HDMP) containing (1) the RLYLRIGRR peptide sequence to bind to lipoteichoic acid (LTA) of gram-positive bacteria, (2) KLVFF for the formation of fibrous structures, and (3) BP for imaging and increasing the hydrophobicity of the structure (**Figure 8a**).[63] HDMP first self-assembled into nanospheres, and it could then transform into nanofibers when it specifically bound to the LTA of *Staphylococcus aureus* (**Figure 8b**). Compared to the control system C-HDMP that could not form nanofibers upon interaction with LTA, HDMP nanoparticles could effectively trap the bacteria due to the formation of fibrous networks (**Figure 8c,d**), thus inhibiting bacterial invasion (**Figure 8e,f**).

3.2.3. Reduced Exocytosis/Efflux

To efficiently accumulate within the tumor, the nanoparticles should not only be internalized into the cells, but they should also be slowly exocytosed from the cells. It has been reported that large NSs typically exhibit a slow exocytosis rate[64] but relatively poor tumor accumulation ability. Thus, the intracellular transformation from small to large structures should be an available way to reduce the efflux of NSs while maintaining the reticuloendothelial system-evading ability of small NSs.

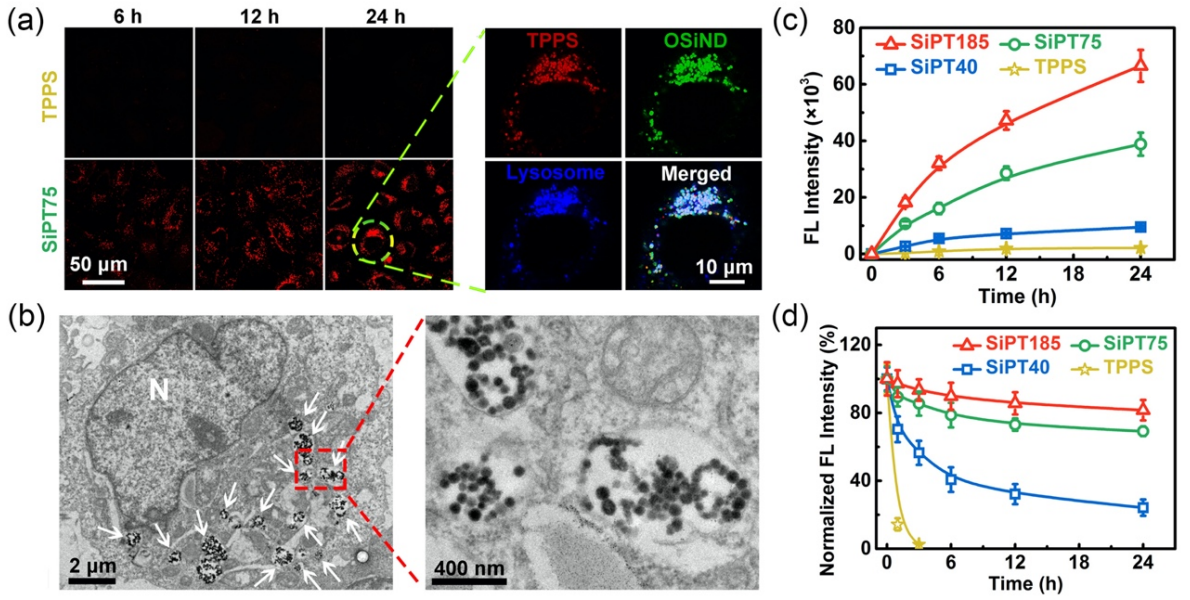

Figure 9. (a) Confocal fluorescence images showing the internalization of free TPPS and SiPT75 in A549/DDP cells and the co-localization of SiPT75 and lysosomes. (b) Bio-TEM images of a SiPT75-treated A549/DDP cell. (c) Time-dependent intracellular TPPS contents after treatments with different formulations. (d) Flow cytometric results showing the anti-efflux performance of the different formulations. Reprinted with permission.[65] Copyright 2020, The Royal Society of Chemistry.

Nam *et al*. found that the formation of AuNP aggregates could block the exocytosis of nanoparticles.[48] In a recent study, Zhang *et al*. designed a series of negatively charged supramolecular nanogels in which all three components, including organosilica nanodots (OSiND), methoxy-PEG-*block*-poly(*L*-glutamic acid sodium salt), and the photosensitizer tetraphenylporphinesulfonate (TPPS), were pH-sensitive.[65] By tuning the ratios of the components, the sizes of the nanogels were 40 (termed SiPT40), 75 (termed SiPT75), and 185 nm (termed SiPT185). Under acidic conditions, the nanogels were less negatively charged and less hydrophilic due to the pH sensitivity of the three components, causing the nanogels to rapidly aggregate in the acidic endosomal/lysosomal environment of *cis*-

dichlorodiammineplatinum(II) (DDP)-resistant A549 cancer cells (A549/DDP cells, **Figure 9a,b**). Compared to free TPPS, the TPPS molecule encapsulated in the nanogels was largely internalized into the cells (**Figure 9c**) and slowly excreted from the cells (**Figure 9d**). This is likely due to the formation of the nanogel aggregates in the acidic organelles that allowed for long-term endosomal/lysosomal retention and the prevention of the efflux of the loaded species.

3.2.4. Controlled Drug Release

Effectively delivering drugs to target tissues/cells and releasing drugs in the target regions are both vital for disease treatment. As stimulus-responsive materials, NSs that can change from small to large NSs have been used for controlled drug release. This type of NSs is typically referred to as an expansile NS. After swelling, the NSs become looser, thus decreasing their interactions with the encapsulated drugs to promote drug release.

For example, Bahadur *et al*. synthesized a block copolymer through the free radical polymerization of 2(pyridin-2-yldisulfanyl)ethyl acrylate and poly(ethylene glycol)methacrylate followed by modification with cyclo(Arg-Gly-Asp-D-Phe-Cys) peptide using the thiol-disulfide exchange reaction.[66] The obtained copolymer could assemble into nanogels capable of loading the anticancer drug DOX. When treated with tris (2-carboxyethyl)phosphine (TCEP) that can break the disulfide bonds in the system, the size of the DOX-loaded nanogels (ND) increased in direct proportion to the incubation time, and the size changed from 115 to 262 nm after 5 h of incubation (**Figure 10a–c**). Furthermore, they found that the DOX release rate from ND was dependent upon the pH value and redox potential of the solution (**Figure 10d**). Fast DOX release was observed under acidic and reductive conditions, possibly due to the looser structure caused by the enlarged size. To construct triple-responsive expansile nanogels, they introduced poly(*N*-isopropyl methacrylamide) with a low critical solution temperature (approximately 43 °C) and pH-sensitive amide groups within the

polymer.[67] The as-prepared system became less hydrophilic when it was dispersed in a redox, acidic, and high-temperature condition. As a result, the size of the nanogels quickly increased from 108 to greater than 1200 nm within 2 h in a reduced and acidic environment at physiological temperature. A silicon phthalocyanine photosensitizer loaded into the nanogels could be quickly released upon swelling of the system.

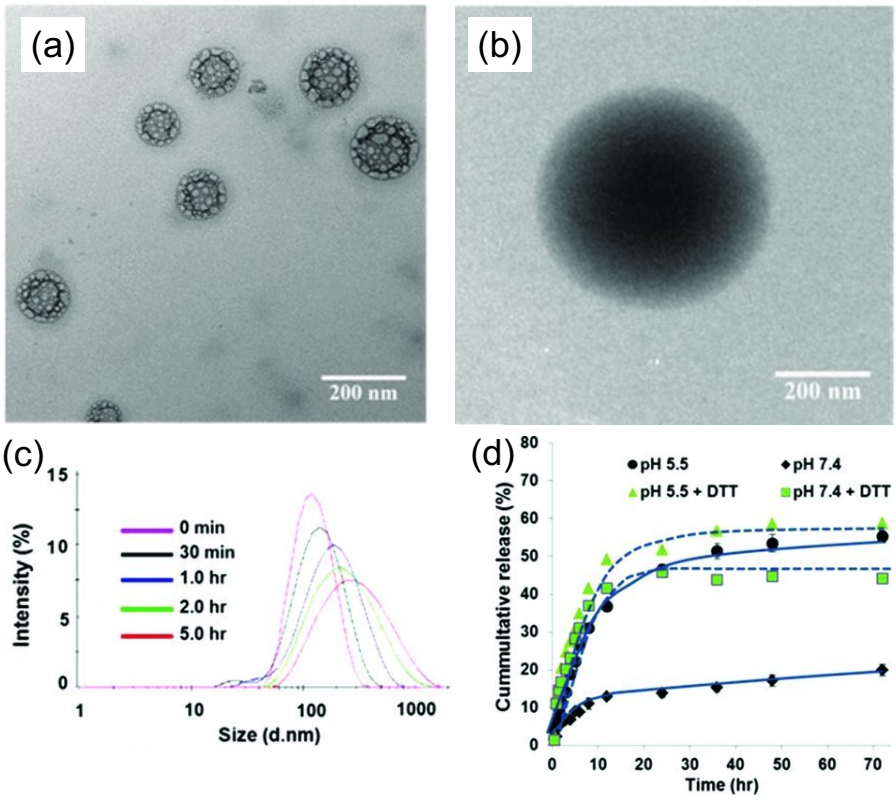

Figure 10. (a,b) TEM images of ND without (b) and with (c) TCEP treatment for 5 h. (c) DLS results of ND treated with TCEP for various periods. (d) DOX release profiles from ND in various solutions. Reprinted with permission.[66] Copyright 2012, Wiley-VCH.

3.2.5. Improved Properties of Disease Theranostics

The size of NSs can significantly impact their chemical and physical properties. After the transformation from a small structure to a large one, NSs may possess different properties that can be used for enhanced disease theranostics. For example, the surface plasmon resonance peaks of well-dispersed AuNPs are typically located in the range of 510–580 nm. However, the

peaks of crosslinked AuNPs or AuNP aggregates exhibit a redshift that can be used for photothermal therapy and photoacoustic imaging. Based on this phenomenon, Cheng *et al*. developed a photo-activated method to crosslink AuNPs that were modified with diazirine (DA)-terminated PEG.[14a] The DA group on the surface of the prepared dAuNPs could transform into carbene in response to 405 nm laser irradiation. The carbene could form covalent bonds with ligands of adjacent dAuNPs through C−C, C−H, O−H, and X−H (X = heteroatom) insertions, ultimately leading to the formation of covalently crosslinked NSs. As expected, the surface plasmon resonance peak of dAuNPs exhibited a significant redshift in response to increasing irradiation period and intensity (**Figure 11a,b**). Meanwhile, the strong NIR absorbance endowed the NSs with enhanced photoacoustic imaging ability and effective photothermal effect (**Figure 11c,d**).

Additionally, it was observed that the T_2 effect of iron oxide particles can be dramatically boosted through particle interaction upon aggregation,[68] and this is favorable for improving the imaging performance of contrast agents. Based on this, Gao *et al*. reported a ^{99m}Tc-labeled Fe_3O_4 nanoprobe that was coated with maleimide-functionalized PEG.[14b] The maleimide group was further conjugated with a peptide composed of Arg-Gly-Asp (RGD) linked to the self-peptide through a disulfide bond. Compared to the nonresponsive probe that did not contain a disulfide bond, the responsive probe possessed a much larger size when incubated with GSH (**Figure 11e,f**). This is due to the ability of GSH to break the disulfide bond of the probe, which resulted in loss of the self-peptide and exposure of the thiol groups of the RGD moiety that allowed them to react with the remaining maleimide residues of adjacent particles. Furthermore, they found that the transverse relaxation rate (R_2) of the responsive probe was rapidly increased by more than 1.82-fold (**Figure 11g**), allowing for an enhanced tumor contrast of more than 3-fold.

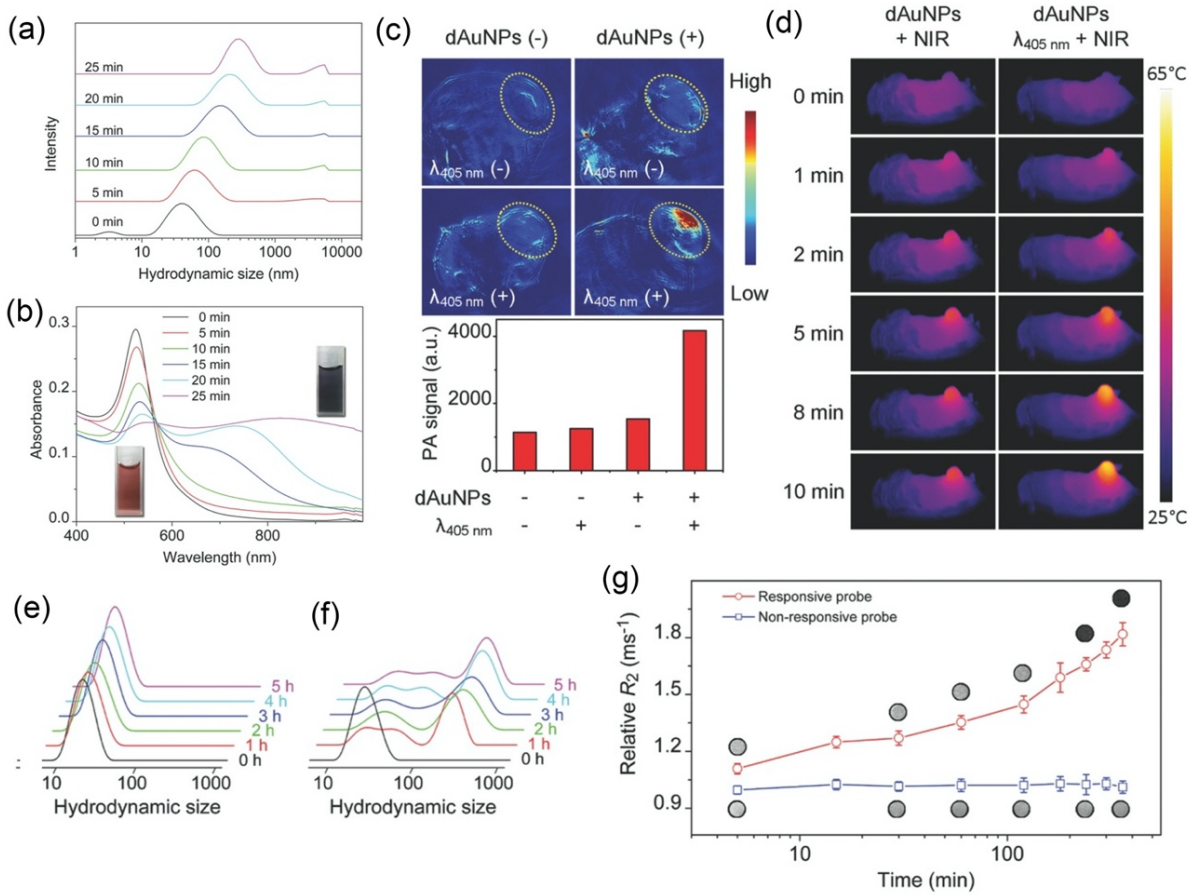

Figure 11. (a) DLS results and (b) absorption spectra of dAuNPs before and after 405 nm irradiation. (c) Photoacoustic images and corresponding photoacoustic signal intensity from the tumor sites of mice receiving various treatments. (d) Photothermal images of tumor-bearing mice after various treatments. Reprinted with permission.[14a] Copyright 2017, Wiley-VCH. (e,f) Time-dependent DLS results of (e) nonresponsive probe and (f) responsive probe incubated with GSH. (g) Time-dependent transverse relaxation rate (R_2) for the responsive probe and nonresponsive probe after incubation with GSH. Reprinted with permission.[14b] Copyright 2017, Wiley-VCH.

4. NSs with Multiple Transformations

In addition to the NSs that undergo only a single-step transformation, NSs that can transform into both small and large NSs have also been designed. These types of NSs can

behave similarly to both size-decreasing and size-increasing NSs and integrate the different advantages of these two types of NSs.

For example, to effectively eradicate a tumor, a drug-loaded nanosystem should possess a suitable size for long-term circulation within the blood and effective accumulation in the tumor through the EPR effect, and they should also act as size-increasing NSs to transform into larger NSs at the tumor site to allow for enhanced tumor accumulation and retention. Then, they should behave as size-deceasing NSs to allow for deep tumor penetration. Based on this, Jia *et al*. reported a pH-responsive and light-activated transformable nanosystem that could effectively inhibit tumor growth and metastasis.[69] This nanosystem was composed of a cytolytic peptide, melittin (MEL), a near-infrared (NIR)-absorbing molecule cypate, and a tumor-targeting polymer HA. The prepared MEL/Cypate@HA complex existed as spherical nanospheres with a size of ~50 nm at neutral pH, transformed into net-like nanofibers in a weakly acidic environment, and then changed into small spherical NSs with a size of ~25 nm that were activated by NIR laser irradiation (**Figure 12a**). As expected, MEL/Cypate@HA could be effectively accumulated in the tumor when compared to the accumulation of free cypate (**Figure 12b**), and these NSs exhibited long-term retention due to their size-increasing properties in the acidic tumor microenvironment (**Figure 12c**). After laser irradiation, the system exhibited deep tumor penetration due to its size-decreasing ability (**Figure 12d**). The nanofibers exerted an inhibitory effect on tumor cell mobility, and this could be used to inhibit the metastatic dissemination of tumor cells to distant organs (**Figure 12e,f**). Similarly, Su *et al*. prepared a size-changeable nanoaircraft (SCNA) possessing a size of 150 nm, and this NS was composed of ultrasmall graphene quantum dots (GQDs, less than 5 nm) and a pH-sensitive polymer *N*-acetyl histidine-functionalized D-α-tocopherol PEG 1000 succinate (HTPGS).[70] Due to the ability of HTPGS to aggregate under weakly acidic conditions, SCNA could increase its size in the tumor region for enhanced tumor retention. Furthermore, NIR irradiation led to

increased temperature in the tumor region due to the presence of GQDs that disassembled the SCNA aggregates into ultrasmall DOX/GQD complexes with a size of 5 nm to improve the tumor penetration ability.

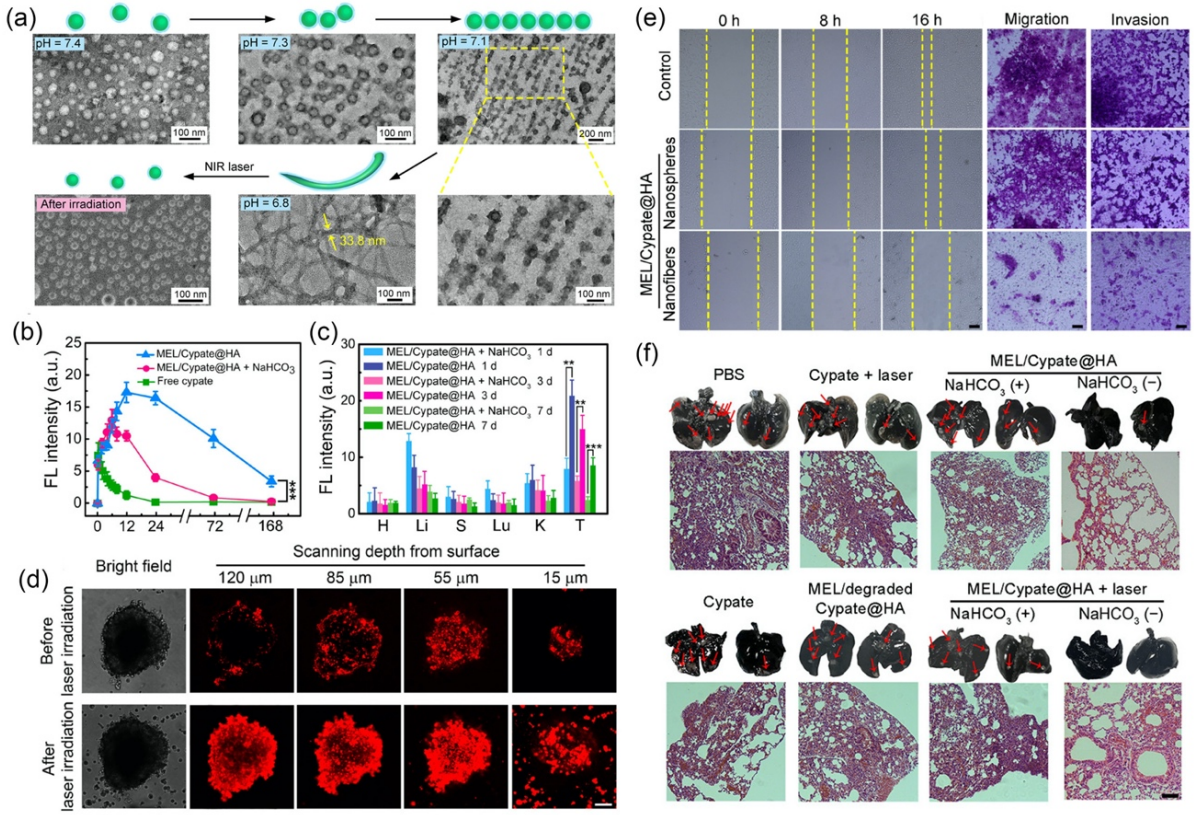

Figure 12. (a) Schematic illustration and TEM images showing the dual transformations of the MEL/Cypate@HA complex induced by the acidic conditions and laser irradiation, respectively. (b) Time-dependent *in vivo* fluorescence intensity in the tumors of the mice after various treatments. (c) Time-dependent *ex vivo* fluorescence intensity of tumors and other organs. (d) Confocal images of MEL/Cypate@HA nanofiber-treated A549 multicellular tumor spheroids before and after laser irradiation. (e) Images of scratch wound healing, migration, and invasion assay results. (f) India ink-stained lungs from the mice after different treatments and corresponding hematoxylin- and eosin-stained tissue slices. Reprinted with permission.[69] Copyright 2019, American Chemical Society.

To simultaneously achieve tumor accumulation and nuclear entry, the size of the NSs should be suitable for accumulation during blood circulation, increase in the tumor region for long-term tumor retention, and finally become smaller than the diameter of nucleopores after internalization into cancer cells. Based on this concept, Guo *et al*. prepared size-changeable polymeric nanosystems ($PELE_{ss}$-DA) in which hydrophobic polylactide (PLA) was selected as the core material and PEG and PEI acted as the corona material.[71] PEI was conjugated to PLA *via* disulfide bonds and functionalized with DMMA, and the presence of DMMA protected the positively charged micelles during blood circulation. After reaching the tumor site, a charge reversal and a size increase occurred in the tumor tissues at low pH, and the nanosystems were subsequently internalized by the tumor cells through electrostatic interactions. This was followed by escape from the lysosomes *via* the proton sponge effect of PEI. The broken disulfide bonds between PLA and PEI resulted in the peeling of the PEI shell, leading to the transformation from large $PELE_{ss}$-DA micelles to small ones for nuclear drug delivery. Inspired by the denaturation and renaturation of proteins, Xiong *et al*. designed an instantaneously transformable NS (DTIG) composed of DOX, tannic acid, and ICG, and this NS possessed proton-triggered hydrophobic−hydrophilic transition capacity and size conversion properties.[72] DTIG possesses a suitable particle size of ~70 nm for blood circulation, and it can be altered into a larger and more hydrophobic NS in the weakly acidic tumor microenvironment to increase their internalization ability into cancer cells. The transformation process was then further accelerated in a more acidic lysosomal environment, and much larger NSs possessing sizes greater than 1.5 μm were formed in the lysosomes, ultimately enabling them to escape from lysosomes by destroying the lysosomal membrane. Finally, the oversize NSs could revert to hydrophilic and small NSs when they moved to the cytoplasm.

To deliver chemotherapeutic agents into the deep tumor, Wang *et al*. designed a core-shell nanocarrier in which the reversible swelling-shrinking core was loaded with an anticancer drug

(DOX) and the degradable gelatin shell was used to encapsulate the autophagy inhibitor 3-methyladenine (3-MA).[73] The gelatin shell could be degraded by the overexpressed MMP-2 in the tumor region to release the encapsulated 3-MA. Then, the exposed small core could become larger upon exposure to the acidic lysosome environment of cancer cells, ultimately resulting in the rapid release of DOX to effectively kill the autophagy-inhibited cancer cells. Interestingly, the core could shrink back in the cytoplasm and the tumor extracellular matrix and cross multiple layers of tumor cells, thus allowing for the effective delivery of the drug into the deep tumor.

5. Conclusion and Perspectives

By integrating the advantages of both large and small NSs, size-transformable NSs have gained much attention for use in disease theranostics. To date, a number of strategies have been developed to construct size-tunable NSs that are responsive to various internal (such as pH, enzyme, ROS, GSH, salt, lactate, and hypoxic environment) or external (such as light and ROS/hyperthermia induced by light irradiation) stimuli. Meanwhile, size-transformable NSs that meet the demands of different sizes under various conditions have been used for deep tumor penetration, prolonged tumor/bacterial retention, controlled drug release, increased cell nucleus influx, decreased cell efflux, and enhanced disease theranostics through the generation of new properties or the improvement of intrinsic properties.

Although many efforts have been dedicated to the design of size-transformable NSs and the development of their biomedical applications, there are still several issues and research directions that can be studied in the future. First, for the size-transformable NSs that are triggered by internal stimuli, the same stimuli may also be present in other tissues and may lead to the undesired transformation of the NSs and off-target disease theranostics. Hence, it is highly desirable to develop changeable systems that can efficiently and specifically transform

at the targeted region. Second, light, the most commonly used external stimulus to control transformation, is difficult to effectively tune the size of NSs in deep tissues due to their intrinsically low tissue light-penetration ability. Thus, developing novel transformable systems based on other external stimuli (such as X-rays, ultrasound, and magnetic fields) that possess strong tumor penetration abilities is urgently needed to improve the transformation ability within deep tissues. Third, after the formation of large structures within the tissues, the NSs would normally become difficult to excrete not only from the targeted tissues but also from the body. Therefore, the long-term biodistribution, biosafety, and biocompatibility of the NSs should be further investigated. Meanwhile, it is possible to redesign the NSs and create the new NSs that are biodegradable or alterable back to small NSs, and these could be easily excreted from the body. Fourth, the effect of the transformation rate on the behavior of NSs should be studied, and it remains challenging to control the transformation rate of the NSs. Fifth, while transformable NSs have been used in some fields, they also possess great potential for use in other biomedical applications such as crossing the BBB, bacterial biofilm penetration, and improvement of internalization ability. Moreover, both small and large NSs possess various advantages in biomedical applications, and transformable NSs can exhibit diverse combination merits due to their ability to integrate and combine the different advantages of small and large NSs. Thus, a more diverse array of transformable NSs should be designed and developed that are capable of exhibiting size-transformable applications in different fields. Finally, in addition to size, other parameters of NSs such as shape, surface charge, flexibility, and hardness can also greatly influence biological actions, including the accumulation efficiency in inflamed cerebral endothelium, transport across the brain endothelium, *in vivo* distribution, and internalization pathways.[74] Although NSs that can change some parameters after stimulus triggering have been prepared,[75] other parameter-changeable NSs should also be designed and their applications should be investigated in the future.

Acknowledgements

This research is supported by the Singapore Agency for Science, Technology and Research (A*STAR) AME IRG grant (A1883c0005), the Singapore Academic Research Fund (RT12/19), the Singapore National Research Foundation Investigatorship (NRF-NRFI2018-03), the National Natural Science Foundation of China (21671136), the Principal Foundation of Shenzhen University (8570700000307), and the Shenzhen Science and Technology Foundation (KQJSCX20180328100401788).

References

[1] a) N. L. Rosi, C. A. Mirkin, *Chem. Rev.* **2005**, *105*, 1547; b) D. Peer, J. M. Karp, S. Hong, O. C. Farokhzad, R. Margalit, R. Langer, *Nat. Nanotechnol.* **2007**, *2*, 751; c) X. Zhang, X. Chen, J. Yang, H. R. Jia, Y. H. Li, Z. Chen, F. G. Wu, *Adv. Funct. Mater.* **2016**, *26*, 5958; d) X. Zhang, X. Chen, H. Y. Wang, H. R. Jia, F. G. Wu, *Adv. Therap.* **2019**, *2*, 1800140; e) Y. W. Lee, R. Mout, D. C. Luther, Y. Liu, L. Castellanos-García, A. S. Burnside, M. Ray, G. Y. Tonga, J. Hardie, H. Nagaraj, R. Das, E. L. Phillips, T. Tay, R. W. Vachet, V. M. Rotello, *Adv. Therap.* **2019**, *2*, 1900041; f) M. Li, H. Zhang, Y. Hou, X. Wang, C. Xue, W. Li, K. Cai, Y. Zhao, Z. Luo, *Nanoscale Horiz.* **2020**, *5*, 202.

[2] a) A. Albanese, P. S. Tang, W. C. Chan, *Annu. Rev. Biomed. Eng.* **2012**, *14*, 1; b) K. Zhang, P. P. Yang, J. P. Zhang, L. Wang, H. Wang, *Chin. Chem. Lett.* **2017**, *28*, 1808; c) Y. Niu, J. Zhu, Y. Li, H. Shi, Y. Gong, R. Li, Q. Huo, T. Ma, Y. Liu, *J. Control. Release* **2018**, *277*, 35; d) W. Yu, R. Liu, Y. Zhou, H. Gao, *ACS Cent. Sci.* **2020**, *6*, 100; e) W. Yu, M. Shevtsov, X. Chen, H. Gao, *Chin. Chem. Lett.* **2020**, *31*, 1366.

[3] B. D. Chithrani, A. A. Ghazani, W. C. W. Chan, *Nano Lett.* **2006**, *6*, 662.

[4] W. Jiang, B. Y. Kim, J. T. Rutka, W. C. Chan, *Nat. Nanotechnol.* **2008**, *3*, 145.

[5] J. Wang, W. Mao, L. L. Lock, J. Tang, M. Sui, W. Sun, H. Cui, D. Xu, Y. Shen, *ACS Nano* **2015**, *9*, 7195.

[6] a) K. R. Raghupathi, R. T. Koodali, A. C. Manna, *Langmuir* **2011**, *27*, 4020; b) Z. Lu, K. Rong, J. Li, H. Yang, R. Chen, *J. Mater. Sci. Mater. Med.* **2013**, *24*, 1465; c) K. Forier, A. S. Messiaen, K. Raemdonck, H. Nelis, S. De Smedt, J. Demeester, T. Coenye, K. Braeckmans, *J. Control. Release* **2014**, *195*, 21.

[7] a) H. S. Choi, W. Liu, P. Misra, E. Tanaka, J. P. Zimmer, B. I. Ipe, M. G. Bawendi, J. V. Frangioni, *Nat. Biotechnol.* **2007**, *25*, 1165; b) F. Alexis, E. Pridgen, L. K. Molnar, O. C. Farokhzad, *Mol. Pharmaceut.* **2008**, *5*, 505.

[8] S. Huo, S. Jin, X. Ma, X. Xue, K. Yang, A. Kumar, P. C. Wang, J. Zhang, Z. Hu, X. J. Liang, *ACS Nano* **2014**, *8*, 5852.

[9] a) M. Nowak, M. E. Helgeson, S. Mitragotri, *Adv. Therap.* **2020**, *3*, 1900073; b) H. Wang, R. Revia, Q. Mu, G. Lin, C. Yen, M. Zhang, *Nanoscale Horiz.* **2020**, *5*, 573.

[10] K. Huang, H. Ma, J. Liu, S. Huo, A. Kumar, T. Wei, X. Zhang, S. Jin, Y. Gan, P. C. Wang, *ACS Nano* **2012**, *6*, 4483.

[11] a) X. Chen, X. Zhang, F. Lin, Y. Guo, F. G. Wu, *Small* **2019**, *15*, 1901647; b) H. H. Ran, X. Cheng, Y. W. Bao, X. W. Hua, G. Gao, X. Zhang, Y. W. Jiang, Y. X. Zhu, F. G. Wu, *J. Mater. Chem. B* **2019**, *7*, 5104.

[12] a) S. Ruan, C. Hu, X. Tang, X. Cun, W. Xiao, K. Shi, Q. He, H. Gao, *ACS Nano* **2016**, *10*, 10086; b) Y. N. Zhang, J. Lazarovits, W. Poon, B. Ouyang, L. N. Nguyen, B. R. Kingston, W. C. Chan, *Nano Lett.* **2019**, *19*, 7226.

[13] N. Oh, J. H. Park, *Int. J. Nanomedicine* **2014**, *9*, 51.

[14] a) X. Cheng, R. Sun, L. Yin, Z. Chai, H. Shi, M. Gao, *Adv. Mater.* **2017**, *29*, 1604894; b) Z. Gao, Y. Hou, J. Zeng, L. Chen, C. Liu, W. Yang, M. Gao, *Adv. Mater.* **2017**, *29*, 1701095.

[15] a) Y. L. Colson, R. Liu, E. B. Southard, M. D. Schulz, J. E. Wade, A. P. Griset, K. A. Zubris, R. F. Padera, M. W. Grinstaff, *Biomaterials* **2011**, *32*, 832; b) T. H. Ku, M. P. Chien, M. P. Thompson, R. S. Sinkovits, N. H. Olson, T. S. Baker, N. C. Gianneschi, *J. Am. Chem. Soc.* **2011**, *133*, 8392; c) R. Tong, H. D. Hemmati, R. Langer, D. S. Kohane, *J. Am. Chem. Soc.* **2012**, *134*, 8848; d) R. Tong, H. H. Chiang, D. S. Kohane, *Proc. Natl. Acad. Sci. U.S.A.* **2013**, *110*, 19048; e) J. Nam, W. G. La, S. Hwang, Y. S. Ha, N. Park, N. Won, S. Jung, S. H. Bhang, Y. J. Ma, Y. M. Cho, M. Jin, J. Han, J. Y. Shin, E. K. Wang, S. G. Kim, S. H. Cho, J. Yoo, B. S. Kim, S. Kim, *ACS Nano* **2013**, *7*, 3388; f) Y. Li, H. Hu, Q. Zhou, Y. Ao, C. Xiao, J. Wan, Y. Wan, H. Xu, Z. Li, X. Yang, *ACS Appl. Mater. Interfaces* **2017**, *9*, 19215; g) N. Zhou, X. Y. Cao, X. W. Du, H. M. Wang, M. Wang, S. Liu, K. Nguyen, K. Schmidt-Rohr, Q. B. Xu, G. L. Liang, B. Xu, *Angew. Chem. Int. Ed.* **2017**, *56*, 2623; h) Y. H. Lai, C. S. Chiang, T. H. Kao, S. Y. Chen, *Int. J. Nanomed.* **2018**, *13*, 3011; i) C. Hu, X. Yang, R. Liu, S. Ruan, Y. Zhou, W. Xiao, W. Yu, C. Yang, H. Gao, *ACS Appl. Mater. Interfaces* **2018**, *10*, 22571; j) Y. Yao, C. Li, F. Liu, P. Zhao, Z. Gu, S. Zhang, *Phys. Chem. Chem. Phys.* **2019**, *21*, 10477; k) R. Liu, Y. An, W. Jia, Y. Wang, Y. Wu, Y. Zhen, J. Cao, H. Gao, *J. Control. Release* **2020**, *321*, 589.

[16] a) M. L. Hans, A. M. Lowman, *Curr. Opin. Solid State Mater. Sci.* **2002**, *6*, 319; b) J. Panyam, V. Labhasetwar, *Adv. Drug Delivery Rev.* **2003**, *55*, 329; c) G. Yang, S. Z. F. Phua, A. K. Bindra, Y. Zhao, *Adv. Mater.* **2019**, *31*, 1805730.

[17] Z. Hai, G. Liang, *Adv. Biosys.* **2018**, *2*, 1800108.

[18] J. Chen, J. Ding, Y. Wang, J. Cheng, S. Ji, X. Zhuang, X. Chen, *Adv. Mater.* **2017**, *29*, 1701170.

[19] S. J. Tseng, I. M. Kempson, K. Y. Huang, H. J. Li, Y. C. Fa, Y. C. Ho, Z. X. Liao, P. C. Yang, *ACS Nano* **2018**, *12*, 9894.

[20] C. Hu, X. Cun, S. Ruan, R. Liu, W. Xiao, X. Yang, Y. Yang, C. Yang, H. Gao, *Biomaterials* **2018**, *168*, 64.

[21] Z. Cong, L. Zhang, S. Q. Ma, K. S. Lam, F. F. Yang, Y. H. Liao, *ACS Nano* **2020**, *14*, 1958.

[22] A. Qi, L. Deng, X. Liu, S. Wang, X. Zhang, B. Wang, L. Li, *J. Biomed. Nanotechnol.* **2017**, *13*, 1386.

[23] H. J. Li, J. Z. Du, X. J. Du, C. F. Xu, C. Y. Sun, H. X. Wang, Z. T. Cao, X. Z. Yang, Y. H. Zhua, S. Nie, J. Wang, *Proc. Natl. Acad. Sci. U.S.A.* **2016**, *113*, 4164.

[24] C. Wong, T. Stylianopoulos, J. Cui, J. Martin, V. P. Chauhan, W. Jiang, Z. Popovic, R. K. Jain, M. G. Bawendi, D. Fukumura, *Proc. Natl. Acad. Sci. U.S.A.* **2011**, *108*, 2426.

[25] S. Ruan, L. Zhang, J. Chen, T. Cao, Y. Yang, Y. Liu, Q. He, F. Gao, H. Gao, *RSC Adv.* **2015**, *5*, 64303.

[26] Q. Chen, J. Chen, C. Liang, L. Feng, Z. Dong, X. Song, G. Song, Z. Liu, *J. Control. Release* **2017**, *263*, 79.

[27] Y. Cai, D. Ni, W. Cheng, C. Ji, Y. Liu, Z. Su, C. Chen, M. Yin, K. Müllen, Y. Wang, *Angew. Chem. Int. Ed.* **2020**, DOI: 10.1002/ange.202001107.

[28] W. Guo, J. Chen, L. Liu, A. S. Eltahan, N. Rosato, J. Yu, D. Wang, J. Chen, M. Bottini, X. J. Liang, *ACS Appl. Mater. Interfaces* **2018**, *10*, 41167.

[29] P. Ray, L. Alhalhooly, A. Ghosh, Y. Choi, S. Banerjee, S. Mallik, S. Banerjee, M. Quadir, *ACS Biomater. Sci. Eng.* **2019**, *5*, 1354.

[30] G. Yang, S. Z. F. Phua, W. Q. Lim, R. Zhang, L. Feng, G. Liu, H. Wu, A. K. Bindra, D. Jana, Z. Liu, Y. Zhao, *Adv. Mater.* **2019**, *31*, 1901513.

[31] Q. Guo, X. He, C. Li, Y. He, Y. Peng, Y. Zhang, Y. Lu, X. Chen, Y. Zhang, Q. Chen, T. Sun, C. Jiang, *Adv. Sci.* **2019**, *6*, 1901430.

[32] G. H. Wang, H. Chen, Y. Y. Cai, L. Li, H. K. Yang, Q. Li, Z. J. He, J. T. Lin, *Mater. Sci. Eng. C Mater. Biol. Appl.* **2018**, *90*, 568.

[33] X. Guo, G. Deng, J. Liu, P. Zou, F. Du, F. Liu, A. T. Chen, R. Hu, M. Li, S. Zhang, Z. Tang, L. Han, J. Liu, K. N. Sheth, Q. Chen, X. Gou, J. Zhou, *ACS Nano* **2018**, *12*, 8723.

[34] X. Chen, X. Zhang, Y. Guo, Y. X. Zhu, X. Liu, Z. Chen, F. G. Wu, *Adv. Funct. Mater.* **2019**, *29*, 1807772.

[35] Y. Chen, X. H. Zhang, D. B. Cheng, Y. Zhang, Y. Liu, L. Ji, R. Guo, H. Chen, X. K. Ren, Z. Chen, Z. Y. Qiao, H. Wang, *ACS Nano* **2020**, *14*, 3640.

[36] A. Schädlich, H. Caysa, T. Mueller, F. Tenambergen, C. Rose, A. Göpferich, J. Kuntsche, K. Mäder, *ACS Nano* **2011**, *5*, 8710.

[37] F. Xu, X. Huang, Y. Wang, S. Zhou, *Adv. Mater.* **2020**, *32*, 1906745.

[38] H. J. Li, J. Z. Du, J. Liu, X. J. Du, S. Shen, Y. H. Zhu, X. Wang, X. Ye, S. Nie, J. Wang, *ACS Nano* **2016**, *10*, 6753.

[39] W. Gao, S. Thamphiwatana, P. Angsantikul, L. Zhang, *Wiley Interdiscip. Rev. Nanomed. Nanobiotechnol.* **2014**, *6*, 532.

[40] Y. Gao, J. Wang, M. Chai, X. Li, Y. Deng, Q Jin, J. Ji, *ACS Nano* **2020**, *14*, 5686.

[41] Z. Cao, Y. Ma, C. Sun, Z. Lu, Z. Yao, J. Wang, D. Li, Y. Yuan, X. Yang, *Chem. Mater.* **2018**, *30*, 517.

[42] a) L. Pan, J. Liu, J. Shi, *Chem. Soc. Rev.* **2018**, *47*, 6930; b) W. H. Chen, G. F. Luo, X. Z. Zhang, *Adv. Mater.* **2019**, *31*, 1802725.

[43] H. Jang, S. R. Ryoo, K. Kostarelos, S. W. Han, D. H. Min, *Biomaterials* **2013**, *34*, 3503.

[44] H. Wang, Y. Li, H. Bai, J. Shen, X. Chen, Y. Ping, G. Tang, *Adv. Funct. Mater.* **2017**, *27*, 1700339.

[45] Q. Hu, W. Sun, Y. Lu, H. N. Bomba, Y. Ye, T. Jiang, A. J. Isaacson, Z. Gu, *Nano Lett.* **2016**, *16*, 1118.

[46] X. Ma, Y. Zhao, *Chem. Rev.* **2014**, *115*, 7794.

[47] Y. Wang, H. Li, Q. Jin, J. Ji, *Chem. Commun.* **2016**, *52*, 582.

[48] J. Nam, N. Won, H. Jin, H. Chung, S. Kim, *J. Am. Chem. Soc.* **2009**, *131*, 13639.

[49] K. Yang, Y. Liu, Y. Wang, Q. Ren, H. Guo, J. B. Matson, X. Chen, Z. Nie, *Biomaterials* **2019**, *223*, 119460.

[50] H. Li, Y. Chen, Z. Li, X. Li, Q. Jin, J. Ji, *Biomacromolecules* **2018**, *19*, 2007.

[51] M. Sun, F. Liu, Y. Zhu, W. Wang, J. Hu, J. Liu, Z. Dai, K. Wang, Y. Wei, J. Bai, W. Gao, *Nanoscale* **2016**, *8*, 4452.

[52] A. P. Griset, J. Walpole, R. Liu, A. Gaffey, Y. L. Colson, M. W. Grinstaff, *J. Am. Chem. Soc.* **2009**, *131*, 2469.

[53] M. Stolzoff, I. Ekladious, A. H. Colby, Y. L. Colson, T. M. Porter, M. W. Grinstaff, *Biomacromolecules* **2015**, *16*, 1958.

[54] X. Fang, W. Jiang, Y. Huang, F. Yang, T. Chen, *J. Mater. Chem. B* **2017**, *5*, 944.

[55] L. Tan, R. Huang, X. Li, S. Liu, Y. M. Shen, Z. Shao, *Carbohydr. Polym.* **2017**, *157*, 325.

[56] a) J. D. Hartgerink, E. Beniash, S. I. Stupp, *Science* **2001**, *294*, 1684; b) V. Castelletto, G. E. Newby, I. W. Hamley, *Macromol. Biosci.* **2008**, *8*, 1182.

[57] P. P. Yang, Q. Luo, G. B. Qi, Y. J. Gao, B. N. Li, J. P. Zhang, L. Wang, H. Wang, *Adv. Mater.* **2017**, *29*, 1605869.

[58] L. Zhang, D. Jing, N. Jiang, T. Rojalin, C. M. Baehr, D. Zhang, W. Xiao, Y. Wu, Z. Cong, J. J. Li, Y. Li, L. Wang, K. S. Lam, *Nat. Nanotechnol.* **2020**, *15*, 145.

[59] C. Zhang, L. H. Liu, W. X. Qiu, Y. H. Zhang, W. Song, L. Zhang, S. B. Wang, X. Z. Zhang, *Small* **2018**, *14*, 1703321.

[60] a) K. Ohkawa, K. I. Minato, G. Kumagai, S. Hayashi, H. Yamamoto, *Biomacromolecules* **2006**, *7*, 3291; b) Q. Mu, G. Lin, Z. R. Stephen, S. Chung, H. Wang, V. K. Patton, R. N. Gebhart, M. Zhang, *Mater. Today* **2020**, DOI: 10.1016/j.mattod.2020.03.005.

[61] G. B. Qi, D. Zhang, F. H. Liu, Z. Y. Qiao, H. Wang, *Adv. Mater.* **2017**, *29*, 1703461.

[62] R. Liu, M. Yu, X. Yang, C. S. Umeshappa, C. Hu, W. Yu, L. Qin, Y. Huang, H. Gao, *Adv. Funct. Mater.* **2019**, *29*, 1808462.

[63] Y. Fan, X. D. Li, P. P. He, X. X. Hu, K. Zhang, J. Q. Fan, P. P. Yang, H. Y. Zheng, W. Tian, Z. M. Chen, L. Ji, H. Wang, L. Wang, *Sci. Adv.* **2020**, *6*, eaaz4767.

[64] B. D. Chithrani, W. C. W. Chan, *Nano Lett.* **2007**, *7*, 1542.

[65] X. Zhang, X. Chen, Y. Guo, H. R. Jia, Y. W. Jiang, F. G. Wu, *Nanoscale Horiz.* **2020**, *5*, 481.

[66] K. C. R. Bahadur, P. Xu, *Adv. Mater.* **2012**, *24*, 6479.

[67] H. He, A. W. Cattran, T. Nguyen, A. L. Nieminen, P. Xu, *Biomaterials* **2014**, *35*, 9546.

[68] S. Laurent, D. Forge, M. Port, A. Roch, C. Robic, L. Vander Elst, R. N. Muller, *Chem. Rev.* **2008**, *108*, 2064.

[69] H. R. Jia, Y. X. Zhu, X. Liu, G. Y. Pan, G. Gao, W. Sun, X. Zhang, Y. W. Jiang, F. G. Wu, *ACS Nano* **2019**, *13*, 11781.

[70] Y. L. Su, T. W. Yu, W. H. Chiang, H. C. Chiu, C. H. Chang, C. S. Chiang, S. H. Hu, *Adv. Funct. Mater.* **2017**, *27*, 1700056.

[71] X. Guo, X. Wei, Y. Jing, S. Zhou, *Adv. Mater.* **2015**, *27*, 6450.

[72] H. Xiong, Z. Wang, C. Wang, J. Yao, *Nano Lett.* **2020**, *20*, 1781.

[73] Y. Wang, Y. Qiu, S. Yin, L. Zhang, K. Shi, H. Gao, Z. Zhang, Q. He, *Autophagy* **2017**, *13*, 359.

[74] a) A. Da Silva-Candal, T. Brownb, V. Krishnan, I. Lopez-Loureiro, P. Ávila-Gómez, A.Pusuluri, A. Pérez-Díaz, C. Correa-Paz, P. Hervella, J. Castillo, S. Mitragotri, F. Campos, *J. Control. Release* **2019**, *309*, 94; b) M. Nowak, T. D. Brown, A. Graham, M. E. Helgeson, S. Mitragotri, *Bioeng. Transl. Med.* **2020**, *5*, e10153; c) K. Xiao, Y. Li, J. Luo, J. S. Lee, W. Xiao, A. M. Gonik, R. G. Agarwal, K. S. Lam, *Biomaterials* **2011**, *32*, 3435; d) Y. Li, X. Zhang, D.

Cao, *Nanoscale* **2015**, *7*, 2758; f) X. Wang, M. Li, Y. Hou, Y. Li, X. Yao, C. Xue, Y. Fei, Y. Xiang, K. Cai, Y. L. Zhao, Z. Luo, *Adv. Funct. Mater.* **2020**, DOI: 10.1002/adfm.202000229.

[75] a) T. Feng, X. Ai, G. An, P. Yang, Y. Zhao, *ACS Nano* **2016**, *10*, 4410; (b) X. C. Jiang, Ji. J. Xiang, H. H. Wu, T. Y. Zhang, D. P. Zhang, Q. H. Xu, X. L. Huang, X. L. Kong, J. H. Sun, Y. L. Hu, K. Li, Y. Tabata, Y. Q. Shen, J. Q. Gao, *Adv. Mater.* **2019**, *31*, 1807591.

Table of Contents Graphic

Size-transformable nanostructures that can inherit the merits of both small and large ones are powerful platforms for enhanced disease theranostics with long-term retention, deep penetration, and rapid clearance. This review introduces various strategies to realize the transformation between large and small nanostructures. The biomedical application potential of this kind of nanostructures is also discussed.

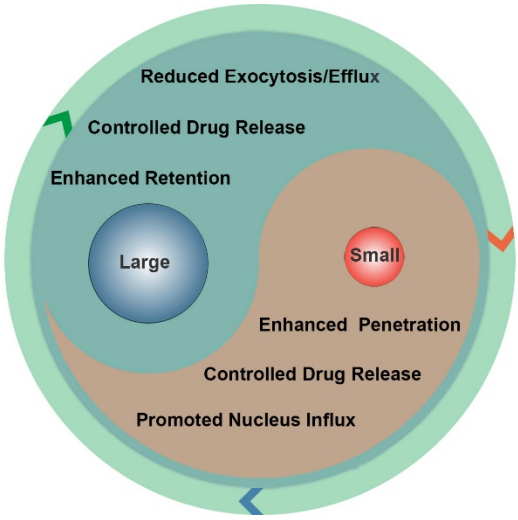

Author biographies and photographs

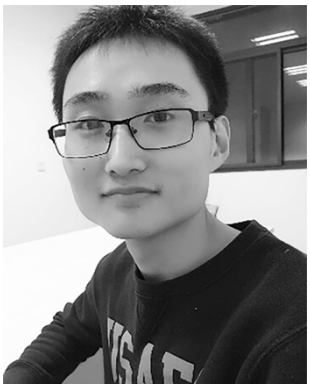

Xiaodong Zhang received his B.Eng. degree and Ph.D. degree in biomedical engineering from Southeast University. He is currently a postdoctoral scholar at Shenzhen University, and is now working with Prof. Yanli Zhao as a visiting researcher. His research interests include the preparation of photoluminescent nanomaterials and their applications in biosensing, bioimaging, and drug delivery.

Xiaokai Chen received her B.Eng. degree and Ph.D. degree in biomedical engineering from Southeast University. She is currently a research fellow at National University of Singapore. She has research experiences in bioimaging and cancer theranostics.

Yanli Zhao is currently a Professor at Nanyang Technological University. He received his B.Sc. degree in chemistry from Nankai University and his Ph.D. degree in physical chemistry there under the supervision of Prof. Yu Liu. He was a postdoctoral scholar with Prof. Sir Fraser Stoddart at University of California Los Angeles and subsequently at Northwestern University. He also conducted postdoctoral research with Prof. Jeffrey Zink at University of California Los Angeles. His current research focuses on integrated nanoparticles for theranostics, and porous materials for gas storage and catalysis.